nature medicine

Article

https://doi.org/10.1038/s41591-024-03362-3

Clinicogenomic landscape of pancreatic adenocarcinoma identifies KRAS mutant dosage as prognostic of overall survival

Received: 26 February 2024

Accepted: 17 October 2024

Published online: 3 January 2025

Check for updates

Anna M. Varghese[1,2,8], Maria A. Perry[3,8], Joanne F. Chou[4], Subhiksha Nandakumar[4,5], Daniel Muldoon[3], Amanda Erakky[2], Amanda Zucker[2], Christopher Fong[5], Miika Mehine[3], Bastien Nguyen[4,5], Olca Basturk[3], Fiyinfolu Balogun[1,2], David P. Kelsen[1,2], A. Rose Brannon[3], Diana Mandelker[3], Efsevia Vakiani[3], Wungki Park[1,2], Kenneth H. Yu[1,2], Zsofia K. Stadler[1,2], Mark A. Schattner[1,2], William R. Jarnagin[2,6], Alice C. Wei[2,6], Debyani Chakravarty[3,5], Marinela Capanu[4], Nikolaus Schultz[4,5,7], Michael F. Berger[3,5,7], Christine A. Iacobuzio-Donahue[2,3,7], Chaitanya Bandlamudi[3,5] ✉ & Eileen M. O'Reilly[1,2] ✉

Nearly all pancreatic adenocarcinomas (PDAC) are genomically characterized by *KRAS* exon 2 mutations. Most patients with PDAC present with advanced disease and are treated with cytotoxic therapy. Genomic biomarkers prognostic of disease outcomes have been challenging to identify. Herein leveraging a cohort of 2,336 patients spanning all disease stages, we characterize the genomic and clinical correlates of outcomes in PDAC. We show that a genomic subtype of *KRAS* wild-type tumors is associated with early disease onset, distinct somatic and germline features, and significantly better overall survival. Allelic imbalances at the *KRAS* locus are widespread. *KRAS* mutant allele dosage gains, observed in one in five (20%) *KRAS*-mutated diploid tumors, are correlated with advanced disease and demonstrate prognostic potential across disease stages. With the rapidly expanding landscape of *KRAS* targeting, our findings have potential implications for clinical practice and for understanding de novo and acquired resistance to RAS therapeutics.

Pancreatic cancer is the third-highest cause of cancer-related mortality and has the lowest 5-year overall survival (OS) rate of all cancer types[1]. For most patients with pancreatic adenocarcinoma (PDAC), the most common pancreatic cancer histology, chemotherapy remains the mainstay of therapy[2–5]. More than 90% of PDACs exhibit activating mutations in *KRAS* hotspot residues, a majority of which have eluded targeted therapeutic approaches until recently[6]. *KRAS* wild-type (WT) tumors are enriched for actionable alterations in mitogen-activated protein kinase (MAPK) pathway genes such as *BRAF*, *NTRK1, NTRK3* and *NRG1* (refs. 7–14).

Superior outcomes are observed in molecularly selected cohorts, such as patients with pathogenic variants in *BRCA1*, *BRCA2* and *PALB2,* and with tumors harboring targetable alterations[2,3,15–18]. Molecular profiling studies have also identified several prognostic features associated with poor outcomes in PDAC[19,20]. In addition, gene expression-based stratification has identified two main subtypes of PDAC, classical and basal-like, that differ in molecular pathology, therapeutic vulnerabilities and outcomes[21–27].

More recently, allelic imbalance (unequal number of maternal and paternal copies) at the *KRAS* locus has been associated with poor

A full list of affiliations appears at the end of the paper. ✉e-mail: bandlamc@mskcc.org; oreillye@mskcc.org

https://doi.org/10.1038/s41591-024-03362-3

Table 1 | MSK-IMPACT PDAC study cohort characteristics

Characteristics	Resectable	BR/LA	Metastatic	Overall
	n=731	*n*=581	*n*=1,024	*n*=2,336
Age at diagnosis (years)	68 (24–91)[a]	66 (32–93)[a]	66 (30–89)[a]	67 (24–93)[a]
Sex				
Male	382 (52%)[b]	293 (50%)[b]	539 (53%)[b]	1,214 (52%)[b]
Female	349 (48%)	288 (50%)	485 (47%)	1,122 (48%)
Genetic ancestry				
European (EUR)	618 (85%)	443 (76%)	828 (81%)	1,889 (81%)
Ashkenazi Jewish (ASJ)	198 (27%)	111 (19%)	263 (26%)	572 (25%)
East Asian (EAS)	42 (5.7%)	27 (4.6%)	44 (4.3%)	113 (4.8%)
African (AFR)	11 (1.5%)	36 (6.2%)	35 (3.4%)	82 (3.5%)
South Asian (SAS)	8 (1.1%)	9 (1.5%)	22 (2.1%)	39 (1.7%)
Admixed/other	52 (7.1%)	66 (11%)	95 (9.3%)	213 (9.1%)
Sample type				
Primary	651 (89%)	473 (81%)	300 (29%)	1,424 (61%)
Metastasis	80 (11%)	108 (19%)	724 (71%)	912 (39%)
MSI-H	4 (0.5%)	3 (0.5%)	3 (0.3%)	10 (0.4%)
TMB-H	10 (1.4%)	11 (1.9%)	14 (1.4%)	35 (1.5%)
Genomic subtype				
KRAS^{MUT}	690 (94%)	557 (96%)	962 (94%)	2,209 (95%)
Other-MAPK^{MUT}	26 (3.6%)	9 (1.5%)	41 (4.0%)	76 (3.3%)
MAPK^{WT}	15 (2.1%)	15 (2.6%)	21 (2.1%)	51 (2.2%)
Resection surgery performed	719 (98%)	221 (38%)	11 (1.1%)	951 (41%)
OS (months)	31 (28, 34)[c]	19 (18, 20)[c]	11 (10, 12)[c]	18 (17, 19)[c]
Clinical curation	*n*=502	*n*=362	*n*=616	*n*=1,480
Tumor location				
Head	356 (71%)	232 (64%)	260 (43%)	848 (58%)
Body/tail	145 (29%)	130 (36%)	339 (57%)	614 (42%)
Smoking history (former/current)	265 (53%)	176 (49%)	288 (47%)	729 (49%)
First-line systemic therapy for metastatic/recurrent disease	288 (57%)	227 (63%)	508 (82%)	1,023 (69%)
FOLFIRINOX	102 (35%)	39 (17%)	248 (49%)	389 (38%)
Gemcitabine/nab-paclitaxel	88 (31%)	107 (47%)	188 (37%)	383 (37%)
Other	98 (34%)	81 (36%)	72 (14%)	251 (25%)

[a]Median (range); [b]*n* (%); [c]median (95% CI). BR/LA, borderline resectable/locally advanced.

outcomes in PDAC[28]. Moreover, *KRAS* mutant allele gains promote aggressive phenotypes in mouse models of pancreatic cancer[29]. Whole-genome doubling (WGD), a hallmark of advanced cancer and a negative prognostic factor for OS, is a key driver promoting allelic imbalances leading to *KRAS* mutant dosage gains[30,31]. However, the prevalence of *KRAS* mutant allele dosage gains in PDAC and its association with disease progression remains poorly understood.

In this study, we leverage germline and somatic profiling of $n = 2,336$ patients to study the genomic and clinical correlates of outcomes for patients with PDAC. We incorporate clinical histories of $n = 1,480$ patients with long-term follow-up. We demonstrate that *KRAS* mutant dosage gains are a hallmark of disease progression and are prognostic of poor outcomes across all stages of PDAC.

Results

MSK-IMPACT PDAC study cohort

This study included $n = 2,336$ patients with PDAC whose tumors were prospectively sequenced as part of standard care at Memorial Sloan Kettering Cancer Center (MSK; Methods; Supplementary Tables 1 and 2). At diagnosis, 31% ($n = 731$) of patients had resectable tumors, 25% ($n = 581$) had borderline resectable/locally advanced tumors and 44% ($n = 1,024$) had metastatic disease (Table 1). Detailed clinical information including lines of treatments, time on treatment and best overall responses were manually curated for 63% ($n = 1,480$) of patients. The majority (61%) of the sequenced specimens were from primary PDAC, and 39% were from distant metastases. Median age at diagnosis was 67 years. Tumor specimens were sequenced to median depth of 606× using the FDA-authorized MSK-IMPACT clinical sequencing assay that encompasses up to 505 cancer genes[32]. Somatic substitutions, insertions, deletions, focal copy number amplifications, homozygous deletions and fusions in select genes were identified using a clinically validated pipeline and annotated using the FDA-recognized precision oncology knowledge base, OncoKB[33,34].

Genomic characteristics of PDACs

Overall, 95% ($n = 2,209$) of tumors harbored oncogenic alterations in *KRAS* (Fig. 1a). Notably, this includes 1% ($n = 22$) of tumors in which *KRAS* mutations were identified with sequencing read evidence below

thresholds for clinical reporting (Methods). Expectedly, tumors WT for *KRAS* (*KRAS*^{WT}) were significantly enriched for oncogenic alterations in other MAPK pathway genes such as *BRAF*, *NRAS*, *NF1*, *NTRK1*, *NTRK3*, *FGFR2*, *ERBB2*, *MAP2K1*, *ROS1*, *MET* and *RAF1* (collectively, 60% in *KRAS*^{WT} versus 7% in *KRAS*^{MUT}, $P = 1.6 \times 10^{-47}$; Fig. 1a). Seven of 26 oncogenic *BRAF* alterations were in-frame deletions between amino acids N486 and P490, which were nearly absent in *BRAF*^{MUT} tumors of melanoma (2 of 749) and thyroid cancer (0 of 473)[14,35] (Extended Data Fig. 1a). Moreover, gain-of-function oncogenic fusions involving MAPK genes were nearly exclusive to *KRAS*^{WT} tumors (3.2% in *KRAS*^{WT} versus 0.04% in *KRAS*^{MUT}, $P = 2 \times 10^{-35}$). Collectively, these other MAPK pathway-altered *KRAS*^{WT} (referred to as other-MAPK^{MUT}) tumors comprise 3% ($n = 76$) of tumors. Finally, 2% ($n = 51$) of tumors were WT for any MAPK pathway alteration (referred to as MAPK^{WT}). Hypothesizing that these MAPK^{WT} tumors may harbor occult MAPK alterations that eluded detection by genomic sequencing, we performed transcriptome sequencing on 11 tumors where sufficient quality material was available. We identified activating fusions involving MAPK pathway genes *BRAF* and *NRG1* in two of 11 tumors (18%), suggesting that a substantial fraction of these tumors may be driven by alterations in non-MAPK pathway genes.

Several significant differences in oncogenic alterations were identified among these three genomic subtypes of PDAC (*KRAS*^{MUT}, other-*MAPK*^{MUT} and *MAPK*^{WT}; Fig. 1a and Extended Data Fig. 1b). *TP53* mutations were significantly more frequent in *KRAS*^{MUT} (78%) compared to other-*MAPK*^{MUT} (38%, $P = 1.4 \times 10^{-9}$) and *MAPK*^{WT} (45%, $P = 1.7 \times 10^{-5}$) tumors. Interestingly, the *TP53* alteration rate among *BRAF*-mutated tumors was indistinguishable from that of *KRAS*^{MUT} tumors, supporting prior observations that *BRAF* mutations phenocopy *KRAS* mutations in pancreas cancers (78% in *KRAS*^{MUT} versus 73% in other-*MAPK*^{MUT}/*BRAF*^{MUT}, $P = 0.6$)[36]. In contrast, *GNAS*, *SMARCB1* and *PIK3CA* alterations were significantly enriched in *MAPK*^{WT} tumors compared to *KRAS*^{MUT} (16% versus 2%, $P = 1.5 \times 10^{-5}$; 8% versus <1%, $P = 2.4 \times 10^{-6}$; 10% versus 2%, $P = 0.002$, respectively). *SMARCB1* loss in *KRAS*^{WT} tumors has previously been associated with the monomorphic anaplastic subtype of undifferentiated carcinomas with rhabdoid features[37]. Here, three of four *SMARCB1*-altered tumors in *MAPK*^{WT} subtype presented with aggressive histologic features of either poor differentiation or high grade, although none exhibited undifferentiated rhabdoid features. *FOXP1* and *CREBBP* alterations were nearly exclusive to other-*MAPK*^{MUT} ($P = 5.3 \times 10^{-5}$ and $P = 1.3 \times 10^{-5}$, respectively, compared to *KRAS*^{MUT}; 0% prevalence in *MAPK*^{WT}). *ARID1A* alterations were enriched in other-*MAPK*^{MUT} compared to *KRAS*^{MUT} tumors (21% versus 8% prevalence, $P = 2.4 \times 10^{-4}$). High tumor mutational burden (10 or more nonsynonymous mutations per megabase, TMB-H) and microsatellite instability-high (MSI-H) tumors were infrequent (1.5% and 0.4%, respectively) and were enriched in *KRAS*^{WT} tumors (TMB-H—6.1% versus 1.8% in *KRAS*^{MUT} tumors, $P = 0.03$; MSI-H—3.7% versus 0.3%, $P = 0.006$; Fig. 1b)[11].

We next explored the association between various clinical characteristics and genomic subtypes of PDAC. Age at diagnosis significantly varied by *KRAS* alteration status. Compared to *KRAS*^{MUT} tumors (median age = 67 years), patients in other-*MAPK*^{MUT} (64 years, $P = 0.03$) and *MAPK*^{WT} (58 years, $P = 2 \times 10^{-4}$) subtypes presented with a significantly earlier age at diagnosis (Fig. 1c and Extended Data Fig. 1c). Patients with *MAPK*^{WT} tumors also had a significantly different ancestry composition compared to patients with *KRAS*^{MUT} (two-sided chi-squared test, $P = 0.004$) or other-*MAPK*^{MUT} tumors ($P = 0.04$), marked by elevated rates of East Asian patients in other-*MAPK*^{MUT} and patients with African ancestry in *MAPK*^{WT} subtypes, indicating the possibility of unrecognized driver alterations in underrepresented patient populations (Fig. 1c). No significant differences were observed in gene-level alteration frequencies across sex or ancestry group (Extended Data Fig. 1d,e).

To evaluate differences in OS across the three genomic subtypes, we used a multivariable Cox proportional hazards model stratified by clinical stage accounting for age, resection status, disease status, sex and genetic ancestry (Methods). We observed that patients with other-*MAPK*^{MUT} and *MAPK*^{WT} tumors had significantly longer OS compared to patients with *KRAS*^{MUT} tumors (*KRAS*^{MUT} versus *MAPK*^{WT}—adjusted hazard ratio (HR_{adj}) = 0.69, CI = 0.48–0.98, $P = 0.041$; *KRAS*^{MUT} versus other-*MAPK*^{MUT}—$HR_{adj} = 0.69$, CI = 0.51–0.93, $P = 0.014$; Fig. 1d,e, top, and Extended Data Table 1). Improved outcomes among *KRAS*^{WT} patients have been attributed to higher prevalence of targetable alterations in this group[14]. After excluding patients who received targeted therapies ($n = 83$), we noted that OS was indistinguishable between patients with *KRAS*^{MUT} and other-MAPK^{MUT} tumors ($HR_{adj} = 0.95$, $P = 0.7$), whereas patients with MAPK^{WT} tumors had significantly better OS ($HR_{adj} = 0.68$, CI = 0.47–0.97, $P = 0.035$; Fig. 1e, bottom, and Extended Data Table 1). This suggests that the well-recognized OS advantage among patients with *KRAS*^{WT} tumors extends beyond those with targetable alterations.

Somatic and clinical characteristics across clinical stages

The stage at diagnosis was similar across genomic subtypes (Fig. 1f). Among other genes, *GNAS*, which is associated with IPMN precursor lesions with improved outcomes over PanIN-derived PDACs, was significantly enriched in resectable tumors (7.9%) while *CDKN2A*/*CDKN2B* alteration rate increased with disease progression ranging from 44% in resectable disease to 60% in metastatic tumors ($P = 6.9 \times 10^{-5}$; Fig. 1g and Extended Data Fig. 2a)[38,39]. No pathway-level differences in alteration rates were observed across disease stages (Extended Data Fig. 2b). Patients with African ancestry presented with more advanced disease (87%) compared to other ancestries (67% in European and 63% in East Asian; Fig. 1h). The location of the tumor in the pancreas was also strongly associated with stage—resectable tumors most commonly arose in the head (71%), while metastatic tumors frequently arose in the body/tail (57%; Fig. 1i and Extended Data Fig. 2d).

Fig. 1 | Somatic alteration landscape in PDAC. a, Oncoprint of somatic oncogenic alterations in selected genes (Methods) across the following three genomic groups: *KRAS*^{MUT}, other-*MAPK*^{MUT} and *MAPK*^{WT}. Tile plot on the left indicates gene-level alteration enrichment in other-*MAPK*^{MUT} and MAPK^{WT} subtypes compared to *KRAS*^{MUT} using two-sided Fisher exact test. An asterisk indicates that *NRG1* was not included in the enrichment analysis as it was profiled only in a subset of samples (Methods). Other MAPK pathway genes include *FGFR1*, *ERBB3*, *FGFR4*, *EGFR*, *RASA1*, *CBL*, *MAPK1*, *ALK*, *MAP2K2*, *ERRFI1*, *FLT3*, *JAK2*, *KIT*, *PDGFRA*, *RAC1*, *RET*, *RRAS2*, *SOS1* and *SPRED1*. **b**, TMB-H and MSI-H prevalence by genomic subtype among tumor samples with ≥30% purity ($n = 1,126$). **c**, Age at diagnosis by genomic subtype with statistical comparison by two-sided Wilcoxon rank sum test ($n = 2,336$). Boxes represent the 25th, 50th (median) and 75th percentiles. Whiskers represent the minimum and maximum values, no further than 1.5× the interquartile range from the respective quartiles, with points beyond this range plotted individually. **d**, Kaplan–Meier curves showing OS for three genomic subtypes (Methods). **e**, Forest plot of multivariable Cox proportional hazards model of OS in overall cohort (top, corresponding to **d**; $n = 2,270$) and among patients who did not receive targeted therapies (bottom; $n = 2,187$). Models were stratified by stage at diagnosis and adjusted for sex, age, ancestry, disease status, resection and interval between diagnosis and sample collection (full model shown in Extended Data Table 1). **f**, Distribution of stage at diagnosis by genomic subtypes ($n = 2,336$). **g**, Prevalence of oncogenic alterations in *GNAS* and *CDKN2A*/*CDKN2B* by stage at diagnosis among tumor samples with purity >30% ($n = 1076$). **h**, Genetic ancestry by stage at diagnosis ($n = 2,336$). **i**, Tumor location (body/tail versus head) by stage ($n = 1,462$). Statistical significance is displayed as nominal *P* value for significant results after multiple test correction by FDR by Wilcoxon rank sum test for **c**, two-sided chi-squared test for **h** and two-sided Fisher's exact test for **b**, **g** and **i**. Error bars represent 95th percentile binomial CI around the mean for **b**, **g** and **i**, and 95th percentile confidence intervals of the HR estimate (colored squares) for **e**. mo, month.

https://doi.org/10.1038/s41591-024-03362-3

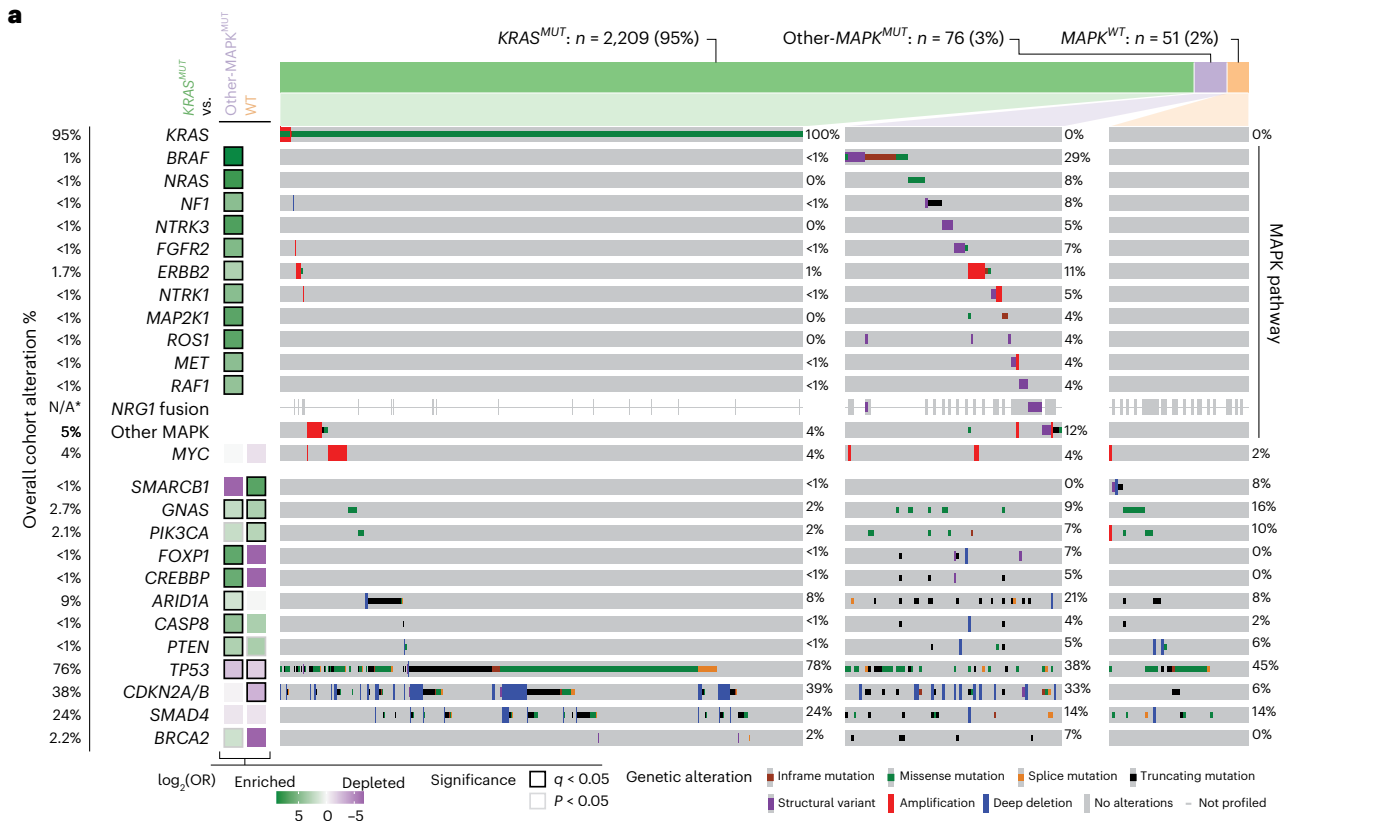

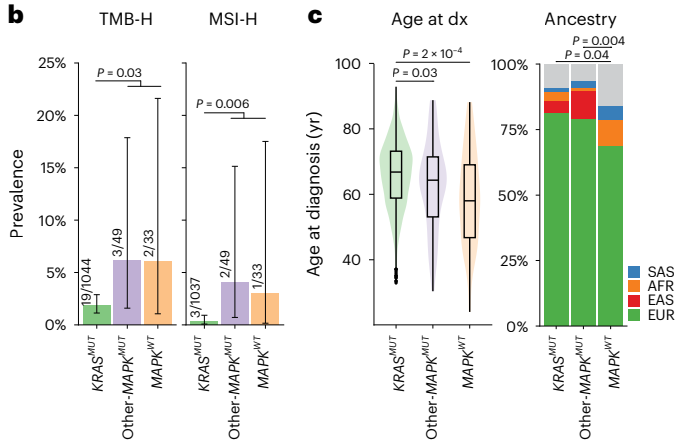

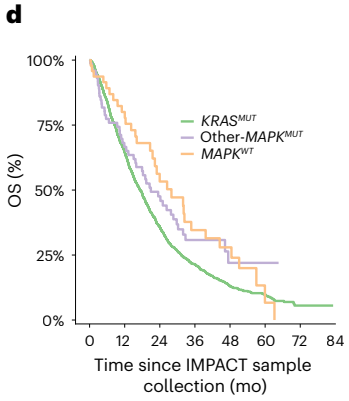

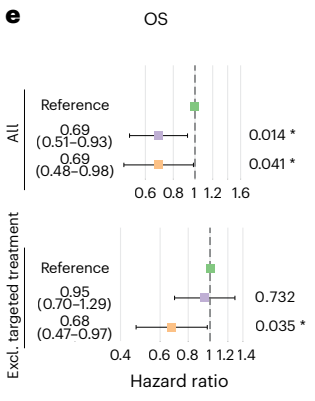

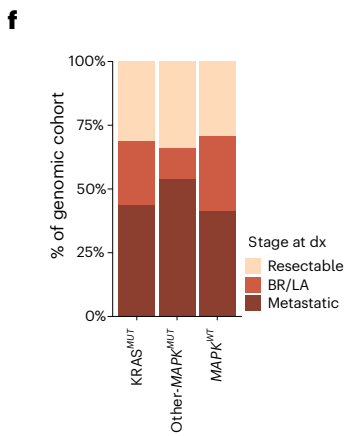

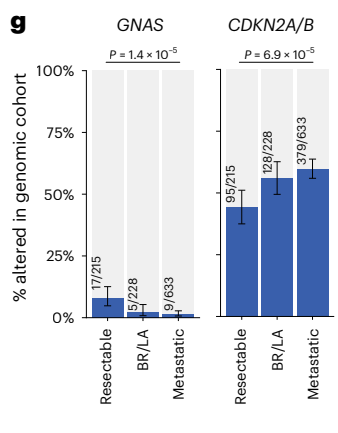

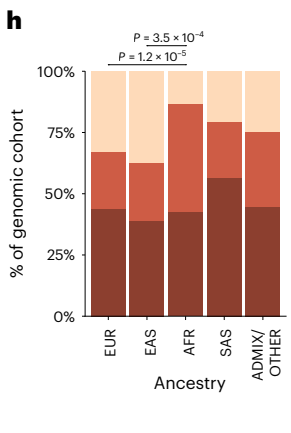

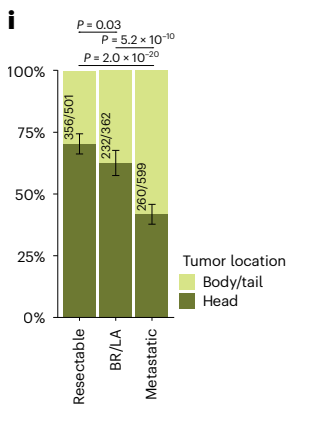

https://doi.org/10.1038/s41591-024-03362-3

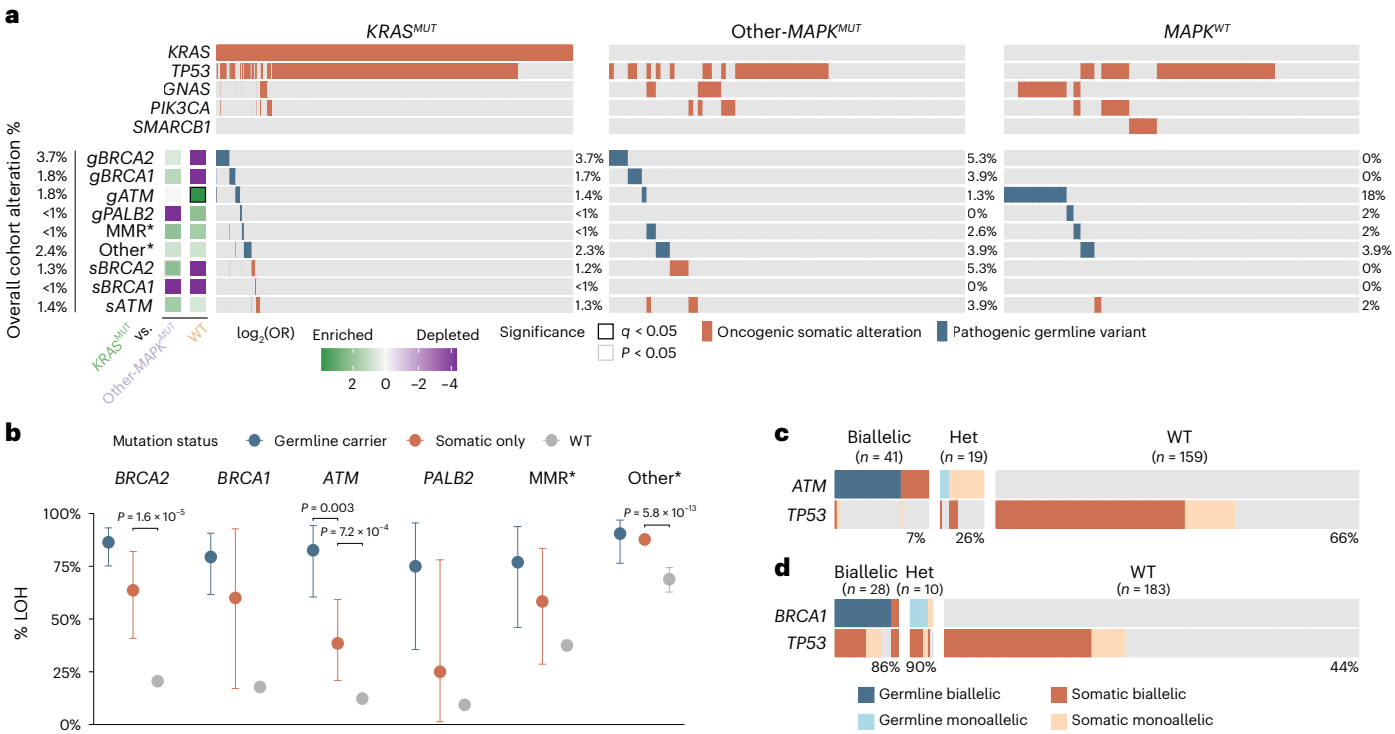

Fig. 2 | Germline alteration landscape in PDAC. a, Oncoprint of pathogenic germline variants and somatic oncogenic alterations by genomic subtype. Displayed *sBRCA2*, *sBRCA1* and *sATM* alterations are exclusively in sporadic tumors without a pathogenic germline variant in these genes. An asterisk indicates that MMR includes *MSH2*, *MSH6*, *MLH1* and *PMS2*. 'Other' includes all other pathogenic variants in high- and moderate-penetrance genes—*BRIP1*, *CDKN2A*, *CHEK2*, *FLCN*, *HOXB13*, *MITF*, *NBN*, *NF1*, *RAD51D*, *SDHA*, *SMARCA4*, *STK11*, *TP53* and *TSC1*. Tiles at left show gene-level enrichment in other-*MAPK*^{MUT} and *MAPK*^{WT} subtypes compared to *KRAS*^{MUT} by two-sided Fisher's exact test. **b**, Rates of loss of heterozygosity (Methods) at *BRCA2*, *BRCA1*, *ATM*, *PALB2*, MMR and other loci (as in **a**) in $n = 1{,}946$ patients with germline pathogenic variants, somatic mutations in sporadic cancers and patients WT for any alteration in corresponding genes (comparisons by two-sided Fisher's exact test). Error bars represent 95th percentile binomial confidence intervals around the mean. **c**, Pattern of germline and somatic *ATM* and *TP53* alterations, with monoallelic or biallelic zygosity status indicated. **d**, Pattern of germline and somatic *BRCA1* and *TP53* alterations, as in **c**.

Germline mutations and concomitant somatic alterations

Ten percent of all patients harbored germline pathogenic mutations in high- and moderate-penetrance genes, including *BRCA2* ($n = 86$, 3.7%), *BRCA1* ($n = 41$, 1.8%), *ATM* ($n = 41$, 1.8%) and *PALB2* ($n = 11$, 0.5%; Fig. 2a). Lynch syndrome with germline mutations in mismatch repair genes *MLH1*, *MSH2*, *MSH6* and *PMS2* was identified in 17 patients (0.7%), of which six (35%) presented with MSI inferred from sequencing[40,41]. Although pathogenic germline variants in *BRCA1*, *BRCA2* and *CHEK2* were more frequent among those with Ashkenazi Jewish (ASJ) ancestry, *ATM* and *PALB2* germline variants were more common among those without ASJ ancestry (Extended Data Fig. 3a). Patients with metastatic disease presented with slightly elevated rates of germline pathogenic variants compared to those with earlier stage disease (12.3% versus 9.6%, $P = 0.01$), driven primarily by an enrichment in *BRCA1*/*BRCA2* alterations in tumors from patients with metastatic disease (Extended Data Fig. 3b). Germline pathogenic variants were more frequent among *MAPK*^{WT} (25%) compared to other-*MAPK*^{MUT} (17%, $P = 0.05$) and *KRAS*^{MUT} (10%, $P = 0.001$). This elevated rate was underpinned by higher prevalence of pathogenic germline mutations in *ATM* (*gATM*) in *MAPK*^{WT} patients compared to *KRAS*^{MUT} (18% versus 1.4%, $P = 2 \times 10^{-6}$; Fig. 2a). Germline *ATM* mutations also co-occurred with somatic *GNAS* mutations, possibly attributed to IPMN-derived PDAC[42,43]. Notably, this increased *gATM* burden in *MAPK*^{WT} tumors was specific to mutations of germline origin as the rate of somatic *ATM* mutations (*sATM*) in *MAPK*^{WT} tumors was not different from the other genomic subtypes ($P > 0.05$; Fig. 2a)[43].

Strong selection for biallelic inactivation through copy number loss of heterozygosity (LOH) was observed in *gBRCA1*, *gBRCA2*, *gPALB2* and *gATM* carriers (Fig. 2b; Methods). The rate of LOH was higher in sporadic tumors with somatic mutations in *BRCA2* and *ATM* compared to tumors without mutations in these genes, but lower compared to LOH rates observed in germline carriers[18,44–46]. As previously reported, *gATM* and *sTP53* mutations were mutually exclusive ($P = 4 \times 10^{-11}$), and *sTP53* alterations and *gBRCA1* mutations co-occurred ($P = 4 \times 10^{-7}$)[44,47]. Interestingly, taking zygosity into account, irrespective of origin of mutation (somatic or germline), tumors with biallelic loss of *ATM* were notably depleted for *sTP53* mutations (Fig. 2c)[44]. In contrast, both monoallelic and biallelic *BRCA1* mutations showed equal co-occurrence with *sTP53* mutations (Fig. 2d).

Mutant allelic imbalance at KRAS locus

We next evaluated the extent to which *KRAS*^{MUT} tumors harbor copy number allelic imbalance (unequal number of maternal and paternal alleles) at *KRAS* locus and mechanism by which allelic imbalance occurs[28] (Fig. 3a). To increase sensitivity and specificity to infer allelic state, we restricted our analysis to $n = 1{,}157$ *KRAS*^{MUT} tumors with sufficiently high-quality copy number fits (Methods). Of these 1,157 tumors, 42% presented with allelic imbalance at *KRAS* locus including focal or arm-level amplifications (4%, $n = 48$), shallow gains (16%, $n = 186$), copy-neutral LOH (CNLOH; 5%, $n = 62$), LOH (11%, $n = 129$) and losses after WGD (5%, $n = 56$; Fig. 3b). Selection for *KRAS* mutant allele was widespread with 93% of all imbalance events preferentially gaining or retaining the mutant allele. One in five (19%) *KRAS*^{MUT} tumors harbored WGD, and the rate of allelic imbalance was substantially higher in WGD tumors (75%) versus non-WGD tumors (30%; Fig. 3c). Consequently, *KRAS*^{MUT} allele gain was more than twice as common in WGD tumors (43% with three or more mutant copies) compared to non-WGD tumors

(20% with two or more mutant copies; Fig. 3d). Moreover, the magnitude of mutant-allele gains also varied by WGD status. Tumors with two or more mutant-allele gains (that is, ≥4 mutant-alleles in WGD and ≥3 mutant-alleles in non-WGD tumors) were substantially more frequent in tumors with WGD (20% versus 6% in non-WGD tumors).

KRAS mutant dosage and prognostic effect

KRAS^{MUT} PDAC tumors with a gain of mutant-allele present with aggressive phenotypes in mice and have worse OS in patients[28,29]. Herein we sought to evaluate the prognostic effect of dosage gains of *KRAS*^{MUT} on OS across disease stages. To mitigate the confounding effects of WGD, a notable negative predictor of OS, we limited our analysis to non-WGD tumors (n = 934; Methods)[30]. In a multivariable Cox model of OS stratified by stage at diagnosis and adjusted for sex, age at diagnosis, genetic ancestry, and time from diagnosis to sample collection, we observed that patients with tumors with any gain of *KRAS*^{MUT} allele had significantly lower OS compared to those with tumors with one mutant allele ($P = 3.5 \times 10^{-7}$, $HR_{adj} = 1.7$, CI = 1.4–2.0; Fig. 3e and Extended Data Table 2). Although no significant difference in OS was observed between patients with tumors harboring two mutant copies (n = 130) and those with 3 or more mutant copies (n = 49) when stratifying by stage, a larger sample size may be required to identify incremental effects of additional dosage gains on prognosis.

KRAS^{MUT} allele dosage gains were more frequent in metastatic tumors (29%) compared to tumors from patients with locally advanced (14%) or resectable (8%) disease and were strongly correlated with advanced disease ($P = 5.7 \times 10^{-11}$, chi-squared trend test; Fig. 3f). This supports prior observations in mouse models with *KRAS* G12D dosage gains, which demonstrated amplified RAS transcriptional programs and exhibited rapid disease progression[29]. Notably, we observe the poor prognostic effect of mutant allele dosage across disease stages (Fig. 3g). Among patients with resectable disease, the median OS was significantly lower in patients with tumors harboring dosage gains of the mutant-allele compared to those whose tumors had one mutant copy (23 months versus 32 months; $HR_{adj} = 2.16$, CI = 1.1–4.3, $P = 0.03$). Similarly, among patients with metastatic disease, *KRAS*^{MUT} dosage gains were associated with 5 months shorter OS compared to patients whose tumors had a single *KRAS*^{MUT} copy (8.5 months versus 13 months; $HR_{adj} = 1.63$, CI = 1.3–2.1, $P = 4.9 \times 10^{-5}$; Extended Data Table 2).

The WT *KRAS* allele in *KRAS*^{MUT} tumors has previously been shown to act as a tumor suppressor[14,48,49]. Tumors adapt during disease progression by losing the WT allele or acquiring additional copies of the mutant allele[50,51]. We therefore hypothesized that patients with *KRAS*^{MUT} tumors with either gain of mutant or with loss of WT should have substantially worse prognosis compared to patients with balanced *KRAS*^{MUT} tumors. However, we observed that only the *KRAS*^{MUT} allele dosage is a notable predictor of poor prognosis, independent of loss or retention of the WT allele. Among patients with *KRAS*^{MUT} tumors that have a single copy of the mutant allele, OS was indistinguishable between patients with tumors that retained the WT allele and those that lost the WT allele (Fig. 3h and Extended Data Table 3). Both groups of patients also demonstrated significantly improved OS compared to patients with *KRAS*^{MUT} tumors with mutant-allele gains, irrespective of WT allele status. However, interestingly, among patients with tumors with *KRAS*^{MUT} dosage gains, patients with tumors with loss of WT had significantly worse OS compared to patients with tumors with WT retained ($HR_{adj} = 1.64$, 95% confidence interval (CI) = 1.1–2.5, $P = 0.016$ for CNLOH with gain-of-mutant as reference). This effect was most prominent among metastatic tumors (Fig. 3i and Extended Data Table 3). Taken together, our findings indicate a synergistic effect of losing the WT allele in tumors with *KRAS*^{MUT} dosage gains in promoting worse disease outcomes.

KRAS mutant allele-specific differences

Over 98% of all codon substitutions in *KRAS* were at G12 (91%) and Q61 (7%) residues (Fig. 4a). Among *KRAS*^{MUT} tumors, G12D (41%) was the most abundant hotspot mutation followed by G12V (32%), and G12R (16%). Fourteen tumors (0.6%) harbored multiple *KRAS* hotspot mutations (Extended Data Fig. 4a,b). No significant differences were observed in *KRAS* variant prevalence by stage at diagnosis, sex, genetic ancestry or age at diagnosis (Fig. 4a and Extended Data Fig. 4c). Patients with G12R-mutant tumors compared to those with G12D-mutant tumors were less likely to have a smoking history (40% versus 55%, $P = 2 \times 10^{-4}$; Extended Data Fig. 4c).

In a multivariable Cox model stratified by stage at diagnosis and accounting for mutant *KRAS* gain, we evaluated the differences in OS among patients with tumors harboring the most common *KRAS* variants (Extended Data Table 4). Patients with *KRAS* G12R-mutant tumors had significantly better OS compared with G12D-driven cancers ($HR_{adj} = 0.78$, CI = 0.67–0.92, $P = 0.003$; Fig. 4b). Among patients with de novo metastatic disease, those with *KRAS* G12D, G12V or G12R mutations did not show significant differences in progression-free survival between those who received first-line FOLFIRINOX compared to gemcitabine-based therapy (Extended Data Fig. 4e,f). Despite the noted differences in functional effects of different *KRAS* alleles, the rates of genome doubling and mutant-allele dosage gains were similar across alleles (Fig. 4a and Extended Data Fig. 4d)[52]. However, in comparing G12D and G12R tumors, *SMAD4* alterations were significantly more common in G12R tumors (30% in G12R versus 21% in G12D, $P = 0.001$), while *ARID1A* alterations were more frequent in G12D tumors (10% in G12D versus 5% in G12R, $P = 0.002$; Fig. 4c)[53].

Clinical actionability in PDAC

Approximately 10% of patients with PDAC harbored standard-of-care biomarkers of response to targeted therapies as defined by OncoKB level 1 (for example, MSI-H, TMB-H and oncogenic MAPK pathway alterations in *NTRK1*, *NTRK3* and *RET*) and level 2 (*KRAS G12C*, *BRCA1*/*BRCA2*, *PALB2*; OncoKB version 4.12, December 2023)[34]. Most strikingly, an additional 78% of patients harbored biomarkers with compelling clinical evidence of response to specific drugs (OncoKB level 3A), nearly all of which (98%) were attributed to *KRAS* G12D/V/R/A/S mutations for which favorable responses to RAS inhibitors have been observed

Fig. 3 | *KRAS* mutant allele dosage gains and their prognostic implications. **a**, Schematic of copy number states as related to mutant copy gain and retention of the WT allele in cases of allelic imbalance. The 'Loss after WGD' state indicates any copy number losses of the minor allele following WGD but excludes complete losses of the minor allele which are considered as CNLOH (Methods). **b**, Overall prevalence of copy number states in *KRAS*^{MUT} tumors. **c**, Prevalence of copy number state with allele selection by WGD status. **d**, Estimated number of gained mutant *KRAS* copies by WGD status. Tumors in which the WT allele was gained, or the mutant allele was lost are not shown here (n = 32, 'WT selection' in **c**). **e**, Kaplan–Meier curves of OS stratified by the number of mutant *KRAS* copies in diploid (non-WGD) *KRAS*^{MUT} tumors excluding tumors with gain of WT allele (n = 865; Extended Data Table 2). **f**, Prevalence of *KRAS* copy number states (left) and mutant copy gain (two or more mutant copies; right) by clinical stage at diagnosis (n = 874). Statistical comparisons show pairwise two-sided Fisher's exact tests. **g**, Kaplan–Meier curves of OS stratified by the number of mutant *KRAS* copies as in **e**, within each clinical stage at diagnosis (Extended Data Table 2). **h**, Kaplan–Meier curves of OS stratified by copy number state in diploid (non-WGD) *KRAS*^{MUT} tumors excluding tumors with gain of WT allele (n = 865; Extended Data Table 3). **i**, Forest plots of multivariable Cox proportional hazards model of OS by *KRAS* copy number state as in **h**, within each clinical stage at diagnosis (n = 865; Extended Data Table 3). Error bars represent 95th percentile binomial CI in **f**, and 95th percentile CI of the HR in **i**. Displayed P values in **e**, **g**–**i** are two-sided nominal P values from multivariable Cox proportional hazards models that include age, sex, ancestry and time from diagnosis to sample collection as covariates. Models for **e** and **h** are stratified by clinical stage at diagnosis (Extended Data Tables 3 and 4). R, resectable; M, metastatic.

https://doi.org/10.1038/s41591-024-03362-3

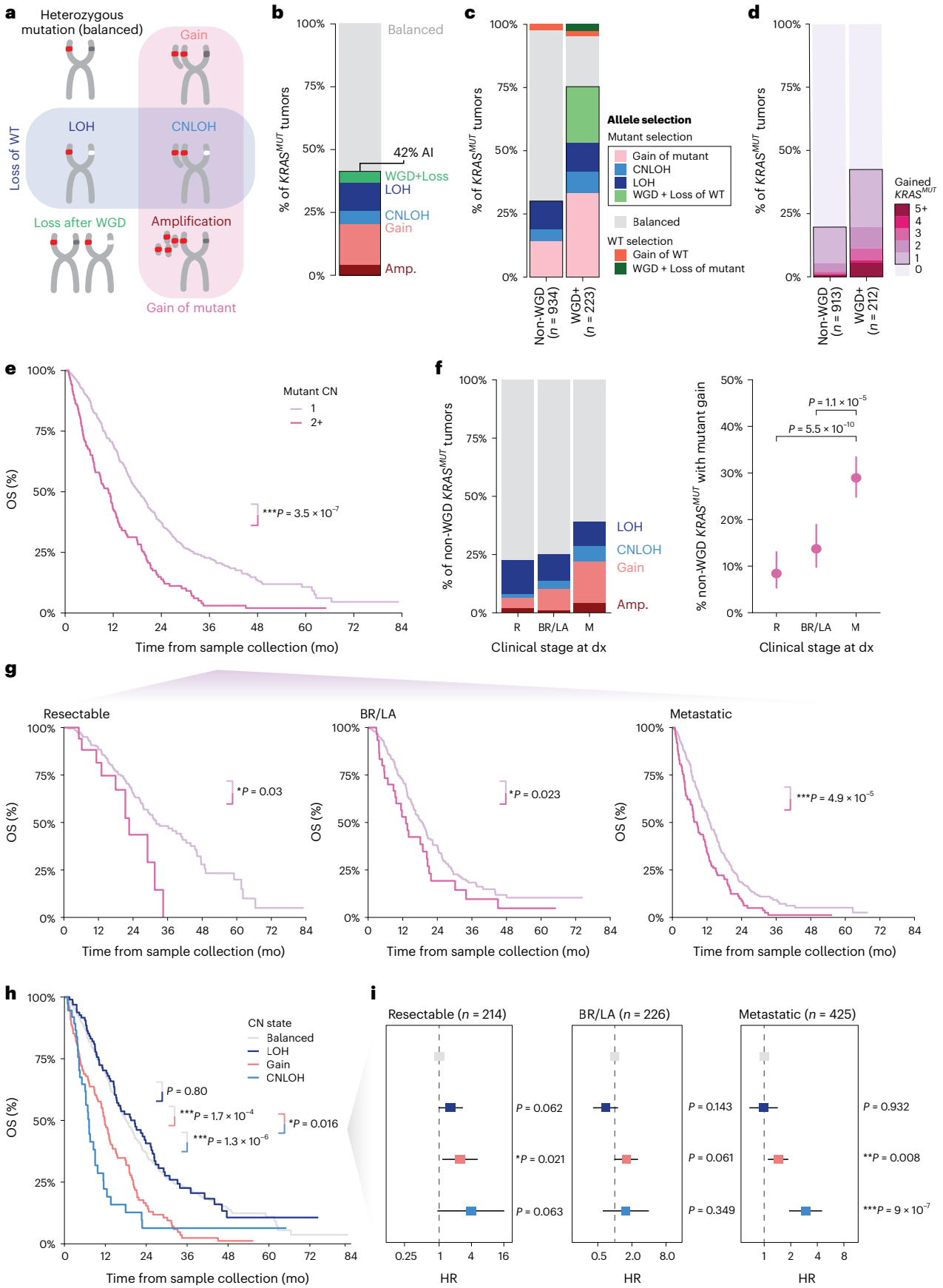

https://doi.org/10.1038/s41591-024-03362-3

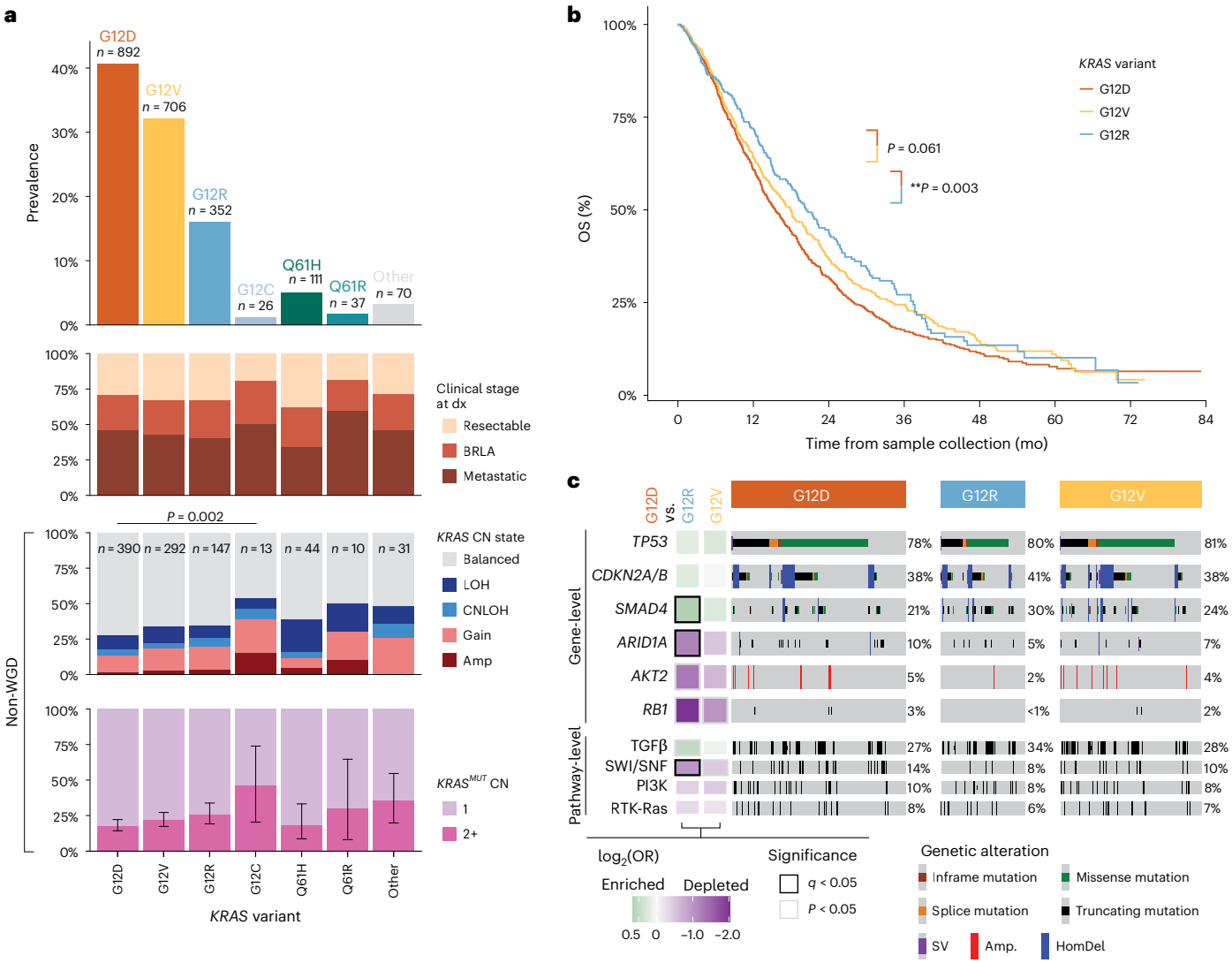

Fig. 4 | Differential genomic and prognostic features of *KRAS* variants. **a**, Top, prevalence of the most common *KRAS* variants among all $KRAS^{MUT}$ tumors. Bottom, disease stage composition, distributions of allelic imbalances and $KRAS^{MUT}$ allele dosage gains across patients with different *KRAS* variants. Allelic imbalances and dosage gains are shown only for non-WGD tumors as indicated. Displayed nominal *P* value denotes statistical comparison of distribution of gene-level copy number state by two-sided chi-squared test. Tumors with multiple driver *KRAS* mutations are not shown here ($n = 14$; Extended Data Fig. 4a,b). Error bars for $KRAS^{MUT}$ CN represent 95th percentile binomial CIs around the mean. **b**, Kaplan–Meier curve of OS among *KRAS* G12D, G12V and G12R variants. Displayed *P* values are nominal two-sided *P* values from a multivariable Cox proportional hazards model stratified by stage at diagnosis and accounting for *KRAS* mutant allele copy number, sex, age, ancestry, disease status and interval from diagnosis to sample collection (Extended Data Table 4). **c**, Oncoprint showing the prevalence of co-occurring *TP53, CDKN2A/CDKN2B, SMAD4, ARID1A, AKT2*, and *RB1* mutations and TGFβ, SWI/SNF, PI3K and RTK–Ras signaling pathway alterations among *KRAS* G12D, G12R and G12V tumors. Tiles on the left indicate pairwise enrichment testing of co-occurring alterations between *KRAS* G12D versus G12R and G12V mutant tumors by two-sided Fisher's exact test.

in recent phase I trials (Fig. 5a)[6,34]. The clinical actionability varied across the genomic subtypes with other-MAPK^{MUT} patients, expectedly, harboring the highest fraction (18%) of OncoKB level 1 alterations (Extended Data Fig. 5). For patients with metastatic PDAC who were fit for systemic therapy, chemotherapy with either a 5-fluorouracil (5-FU) or gemcitabine-based backbone was administered (Table 1 and Fig. 5b)[5]. Treatment selection reflected changes in standard-of-care guidelines over the course of the study[54].

We next evaluated molecular correlates of response to poly-ADP ribose polymerase inhibitors (PARPi). In our clinically curated cohort, $n = 29$ patients with stage IV disease at diagnosis received PARPi therapy at any time during their treatment. Of these, 25 patients had germline ($n = 23$) or somatic ($n = 2$) mutations in *BRCA2* ($n = 18$), *BRCA1* ($n = 6$) and *PALB2* ($n = 1$; Fig. 5c). Twenty-eight of 29 patients had $KRAS^{MUT}$ tumors, 4 of which also had mutant allele dosage gains. Overall, 38% (11 of 29) of patients received PARPi therapy for more than six months (median 17 months; range = 8–56). Ten of 11 (91%) patients had $BRCA2^{MUT}$; the remaining patient had a $BRCA1^{WT}/BRCA2^{WT}$ and $MAPK^{WT}$ tumor with a *BAP1* loss-of-function fusion. While all ten *BRCA2*-mutant tumors deriving benefit from PARPi (defined as >6 months on treatment) had biallelic inactivation, no benefit was observed among six other *BRCA2*-mutant tumors with biallelic losses, suggesting that biallelic loss of *BRCA1*/*BRCA2* is an important but insufficient biomarker alone of response to PARPi[55].

We next sought to identify the genomic correlates of OS in $KRAS^{MUT}$ patients with de novo metastatic disease who received first-line standard-of-care chemotherapy ($n = 304$, median OS = 10.5 months; Methods; Fig. 5d). We evaluated associations between genes altered in at least 3% of patients ($n = 13$ genes) and OS using a multivariable Cox regression model accounting for sex, age, ancestry and interval

https://doi.org/10.1038/s41591-024-03362-3

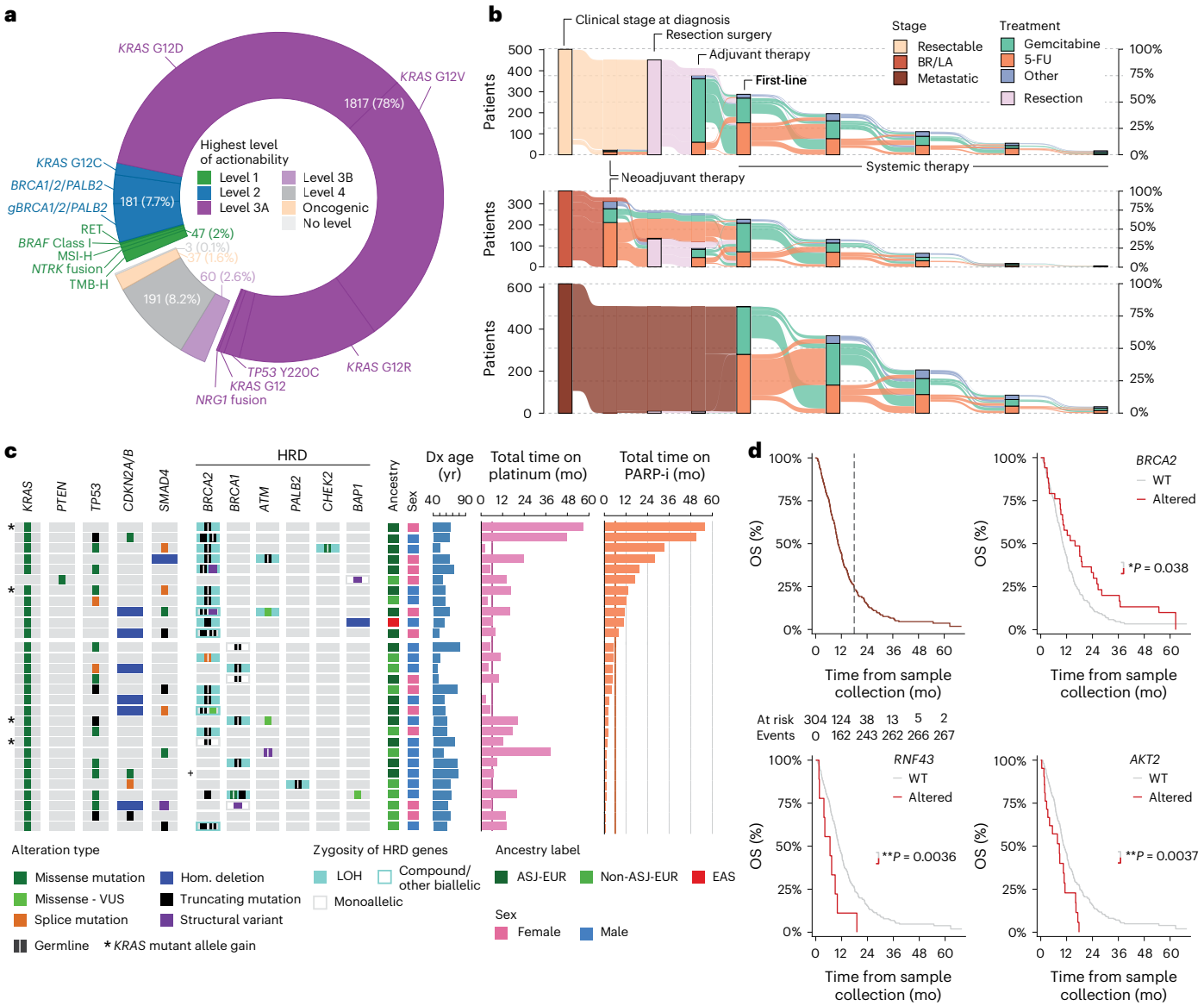

Fig. 5 | Clinically actionable alterations and treatment landscape. **a**, Highest OncoKB level of evidence by patient, with actionable (levels 1, 2 and 3A) alterations labeled. **b**, Alluvial diagram of treatment sequence for all 1,480 patients with treatment annotation by clinical stage at diagnosis showing prevalence of neoadjuvant therapy, resection surgery, adjuvant therapy and up to 5 rounds of systemic therapy. Different lines of treatment are shown on the *x* axis. **c**, Clinicogenomic characterization of $n = 29$ patients who were metastatic at presentation and received PARP-inhibitor therapy as part of systemic treatment. Cumulative times on PARP-inhibitor therapy and platinum therapy are shown as bar charts, along with demographic information (age at diagnosis, sex and genetic ancestry), germline and somatic alterations in HRD genes with associated zygosity, and somatic alterations in other commonly altered genes or genes of interest. The patient marked with a plus (+) received PARP-inhibitor therapy to target a germline *RAD50* mutation (not shown). **d**, OS for $n = 304$ patients who were metastatic at presentation and received either 5-FU or gemcitabine-based first-line treatments (top left). Top-right, bottom-left and bottom-right, Kaplan–Meier curves of OS by alteration status of indicated genes. *P* values are nominal two-sided *P* values from a multivariable Cox model that accounts for sex, age, ancestry and interval from diagnosis to sample collection for each gene (Methods; Extended Data Table 5).

from diagnosis to biospecimen collection (Methods; Extended Data Table 5). Only patients with *BRCA2* alterations (including germline carriers) showed modestly improved outcomes ($HR_{adj} = 0.66$, 95% CI = 0.44–0.98, $P = 0.038$), in line with the established response to platinum therapy[16,18,56] (Fig. 5d). After correcting for multiple hypothesis testing, alterations in two genes remained significant. Both were associated with a significantly shorter OS—*RNF43* ($HR_{adj} = 2.79$, 95% CI = 1.40–5.56, $P_{adj} = 0.047$; median OS = 6.6 months $RNF43^{MUT}$ versus 10.8 months $RNF43^{WT}$) and *AKT2* amplifications ($HR_{adj} = 2.03$, 95% CI = 1.26, 3.29, $P_{adj} = 0.048$; median OS = 8.6 months in $AKT2^{MUT}$ versus 10.8 months in $AKT2^{WT}$). Although not commonly altered in PDAC (<5% in this cohort), *RNF43* loss-of-function activity has been shown to be *KRAS* dependent[57]. While *KRAS* mutant gains were more frequent in $RNF43^{MUT}$ tumors, this did not reach statistical significance in our cohort (67% of $RNF43^{MUT}$ tumors had *KRAS* mutant gains versus 30% in $RNF43^{WT}$, $P = 0.2$). Together, these results suggest that prognosis in patients with PDAC is most linked to *KRAS* mutation and dosage in the majority of patients, and that somatic alterations in other genes do not explain the wide variation in response to standard therapies.

Discussion

Herein we study the detailed clinicogenomic profiles of $n = 2{,}336$ patients to characterize prognostic biomarkers guiding clinical outcomes in PDAC. Compared to prior studies, our cohort has several

unique strengths including many molecularly profiled metastatic tumors, detailed clinical histories for two-thirds of patients, and matched tumor and normal sequencing that allowed for incorporation of germline results and robust inference of allele-specific copy number states at the mutated loci. Collectively, these strengths enabled improved classification of PDAC into genomic subtypes and the demonstration of prognostic potential of mutant allele dosage gains in $KRAS^{MUT}$ tumors across all disease stages.

Our findings have several clinical implications. The predictive role of *KRAS* mutant dosage gains in impacting antitumor response and therapeutic outcomes remains unknown, although we expect it to be important. As many RAS-targeted therapies are advancing in clinical trials, it is imperative to conduct analyses to evaluate whether *KRAS* mutant dosage has a role in mediating efficacy as well as depth and duration of response to treatment. Findings from such studies may provide impetus for future trials to stratify patients by *KRAS* mutant dosage in evaluating therapeutic outcomes. For example, randomized clinical trials that evaluate patients with *KRAS* mutant dosage gains in both the intervention as well as control arms are key to evaluate response to RAS inhibitors as well as current standard-of-care therapies. Second, shallow gains of *KRAS* mutant alleles, including single-copy gains, which are associated with poor outcomes and can potentially guide care, are currently not reported by any clinical sequencing assays. There is an imminent need for evaluation, standardization and incorporation of these low-level gains into reports for clinical interpretation. Third, acknowledging the challenge of small biopsy specimens in the diagnosis and management of patients with PDAC, it is essential to understand whether circulating tumor DNA can provide a noninvasive means of assessing *KRAS* mutant dosage and whether sequential analyses could provide a dynamic and real-time assessment to inform response and resistance.

Although PDACs are genomically grouped by *KRAS* status, our data argue that the $KRAS^{WT}$ tumors comprise two distinct molecular groups stratified by whether or not they harbor oncogenic alterations in other MAPK pathway genes. The other-$MAPK^{MUT}$ and $MAPK^{WT}$ subtypes comprise 3% and 2% of all PDACs, respectively, and reveal distinct etiologic and molecular factors underpinning tumorigenesis. However, further molecular and biochemical studies that measure the activity of Ras–ERK signaling as well as the upregulation of downstream components including *MYC* or *YAP* are needed to establish MAPK independence among these $MAPK^{WT}$ tumors[58].

In this large clinicogenomically characterized cohort of patients with PDAC, several important limitations need highlighting. Patients were evaluated and treated at a major referral center for PDAC with inherent biases of fitness, age and other characteristics. With current trends of increasing incidence of early-onset PDAC, especially in younger women, these characteristics are important to note[59,60]. We report a high proportion of patients undergoing resection of primary pancreatic cancer, 41%, which is higher than the broader population of all patients with PDAC (Table 1). Relatedly, only 15% of our cohort was non-European, highlighting the need for these results to be evaluated in subgroups with greater ethnic and racially diverse populations. This study primarily focuses on genomic features derived from MSK-IMPACT. Additional transcriptomic assessments are needed to fully characterize pathway-level activity and to identify the relationship between genomic biomarkers described herein and previously described transcriptomic subtypes (classical and basal) that have been associated with prognosis and for which predictive implications are under evaluation in clinical trials (NCT04469556)[25]. Given the prognostic potential of both *KRAS* dosage and the basal-like transcriptomic subtype, a comprehensive analysis of subtyping is needed to determine whether these are indicative of the same or independent pathways of tumor progression.

Comprehensive analysis of germline and somatic alterations is critically important in PDAC and both have therapeutic implications. Additionally, integration with demographic and clinical information is required to link understanding of underlying tumor biology with treatment implications and outcomes. We identify distinct molecular and clinical features of $KRAS^{MUT}$, other-$MAPK^{MUT}$ and $MAPK^{WT}$ genomic subtypes and further stratify $KRAS^{MUT}$ tumors by allele-specific copy number. Collectively, these findings demonstrate that increased *KRAS* mutant allele dosage is an important negative prognostic feature that will need to be integrated into clinical practice as we move into the era of RAS-directed therapeutics for PDAC.

Online content

Any methods, additional references, Nature Portfolio reporting summaries, source data, extended data, supplementary information, acknowledgements, peer review information; details of author contributions and competing interests and statements of data and code availability are available at https://doi.org/10.1038/s41591-024-03362-3.

References

1. Siegel, R. L., Giaquinto, A. N. & Jemal, A. Cancer statistics, 2024. *CA Cancer J. Clin.* **74**, 12–49 (2024).
2. Conroy, T. et al. FOLFIRINOX versus gemcitabine for metastatic pancreatic cancer. *N. Engl. J. Med.* **364**, 1817–1825 (2011).
3. Von Hoff, D. D. et al. Increased survival in pancreatic cancer with nab-paclitaxel plus gemcitabine. *N. Engl. J. Med.* **369**, 1691–1703 (2013).
4. Wainberg, Z. A. et al. NAPOLI-3: a randomized, open-label phase 3 study of liposomal irinotecan+5-fluorouracil/leucovorin+oxaliplatin (NALIRIFOX) versus nab-paclitaxel+gemcitabine in treatment-naive patients with metastatic pancreatic ductal adenocarcinoma (mPDAC). *J. Clin. Oncol.* **41**, LBA661–LBA661 (2023).
5. Park, W., Chawla, A. & O'Reilly, E. M. Pancreatic cancer: a review. *JAMA* **326**, 851 (2021).
6. Arbour, K. C. et al. 652O Preliminary clinical activity of RMC-6236, a first-in-class, RAS-selective, tri-complex RAS-MULTI(ON) inhibitor in patients with KRAS mutant pancreatic ductal adenocarcinoma (PDAC) and non-small cell lung cancer (NSCLC). *Ann. Oncol.* **34**, S458 (2023).
7. Drilon, A. et al. Efficacy of larotrectinib in TRK fusion-positive cancers in adults and children. *N. Engl. J. Med.* **378**, 731–739 (2018).
8. Guan, M. et al. Molecular and clinical characterization of BRAF mutations in pancreatic ductal adenocarcinomas (PDACs). *J. Clin. Oncol.* **36**, 214–214 (2018).
9. Li, H.-S., Yang, K. & Wang, Y. Remarkable response of *BRAF* V600E-mutated metastatic pancreatic cancer to BRAF/MEK inhibition: a case report. *Gastroenterol. Rep.* **10**, goab031 (2022).
10. Schram, A. M. et al. Zenocutuzumab, a HER2xHER3 bispecific antibody, is effective therapy for tumors driven by *NRG1* gene rearrangements. *Cancer Discov.* **12**, 1233–1247 (2022).
11. Philip, P. A. et al. Molecular characterization of *KRAS* wild-type tumors in patients with pancreatic adenocarcinoma. *Clin. Cancer Res.* **28**, 2704–2714 (2022).
12. Le, D. T. et al. PD-1 blockade in tumors with mismatch-repair deficiency. *N. Engl. J. Med.* **372**, 2509–2520 (2015).
13. Topham, J. T. et al. Integrative analysis of KRAS wildtype metastatic pancreatic ductal adenocarcinoma reveals mutation and expression-based similarities to cholangiocarcinoma. *Nat. Commun.* **13**, 5941 (2022).
14. Singh, H. et al. Oncogenic drivers and therapeutic vulnerabilities in KRAS wild-type pancreatic cancer. *Clin. Cancer Res.* **29**, 4627–4643 (2023).
15. Pishvaian, M. J. et al. Overall survival in patients with pancreatic cancer receiving matched therapies following molecular profiling: a retrospective analysis of the Know Your Tumor registry trial. *Lancet Oncol.* **21**, 508–518 (2020).

16. Golan, T. et al. Maintenance olaparib for germline BRCA-mutated metastatic pancreatic cancer. *N. Engl. J. Med.* **381**, 317–327 (2019).
17. O'Reilly, E. M. et al. Randomized, multicenter, phase II trial of gemcitabine and cisplatin with or without veliparib in patients with pancreas adenocarcinoma and a germline *BRCA*/*PALB2* mutation. *J. Clin. Oncol.* **38**, 1378–1388 (2020).
18. Park, W. et al. Genomic methods identify homologous recombination deficiency in pancreas adenocarcinoma and optimize treatment selection. *Clin. Cancer Res.* **26**, 3239–3247 (2020).
19. Blackford, A. et al. *SMAD4* gene mutations are associated with poor prognosis in pancreatic cancer. *Clin. Cancer Res.* **15**, 4674–4679 (2009).
20. Crane, C. H. et al. Phase II trial of cetuximab, gemcitabine, and oxaliplatin followed by chemoradiation with cetuximab for locally advanced (T4) pancreatic adenocarcinoma: correlation of *Smad4(Dpc4)* immunostaining with pattern of disease progression. *J. Clin. Oncol.* **29**, 3037–3043 (2011).
21. Raphael, B. J. et al. Integrated genomic characterization of pancreatic ductal adenocarcinoma. *Cancer Cell* **32**, 185–203.e13 (2017).
22. Lowery, M. A. et al. Real-time genomic profiling of pancreatic ductal adenocarcinoma: potential actionability and correlation with clinical phenotype. *Clin. Cancer Res.* **23**, 6094–6100 (2017).
23. Bailey, P. et al. Genomic analyses identify molecular subtypes of pancreatic cancer. *Nature* **531**, 47–52 (2016).
24. Collisson, E. A. et al. Subtypes of pancreatic ductal adenocarcinoma and their differing responses to therapy. *Nat. Med.* **17**, 500–503 (2011).
25. Moffitt, R. A. et al. Virtual microdissection identifies distinct tumor- and stroma-specific subtypes of pancreatic ductal adenocarcinoma. *Nat. Genet.* **47**, 1168–1178 (2015).
26. Waddell, N. et al. Whole genomes redefine the mutational landscape of pancreatic cancer. *Nature* **518**, 495–501 (2015).
27. Puleo, F. et al. Stratification of pancreatic ductal adenocarcinomas based on tumor and microenvironment features. *Gastroenterology* **155**, 1999–2013.e3 (2018).
28. Bielski, C. M. et al. Widespread selection for oncogenic mutant allele imbalance in cancer. *Cancer Cell* **34**, 852–862.e4 (2018).
29. Mueller, S. et al. Evolutionary routes and KRAS dosage define pancreatic cancer phenotypes. *Nature* **554**, 62–68 (2018).
30. Bielski, C. M. et al. Genome doubling shapes the evolution and prognosis of advanced cancers. *Nat. Genet.* **50**, 1189–1195 (2018).
31. Chan-Seng-Yue, M. et al. Transcription phenotypes of pancreatic cancer are driven by genomic events during tumor evolution. *Nat. Genet.* **52**, 231–240 (2020).
32. Cheng, D. T. et al. Memorial Sloan Kettering-Integrated Mutation Profiling of Actionable Cancer Targets (MSK-IMPACT): a hybridization capture-based next-generation sequencing clinical assay for solid tumor molecular oncology. *J. Mol. Diagn.* **17**, 251–264 (2015).
33. Zehir, A. et al. Mutational landscape of metastatic cancer revealed from prospective clinical sequencing of 10,000 patients. *Nat. Med.* **23**, 703–713 (2017).
34. Chakravarty, D. et al. OncoKB: a precision oncology knowledge base. *JCO Precis. Oncol.* **2017**, PO.17.00011 (2017).
35. Foster, S. A. et al. Activation mechanism of oncogenic deletion mutations in BRAF, EGFR, and HER2. *Cancer Cell* **29**, 477–493 (2016).
36. Collisson, E. A. et al. A central role for RAF→MEK→ERK signaling in the genesis of pancreatic ductal adenocarcinoma. *Cancer Discov.* **2**, 685–693 (2012).
37. Agaimy, A. et al. Pancreatic undifferentiated rhabdoid carcinoma: KRAS alterations and SMARCB1 expression status define two subtypes. *Mod. Pathol.* **28**, 248–260 (2015).
38. Hosoda, W. et al. GNAS mutation is a frequent event in pancreatic intraductal papillary mucinous neoplasms and associated adenocarcinomas. *Virchows Arch.* **466**, 665–674 (2015).
39. McGinnis, T. et al. Survival outcomes of pancreatic intraepithelial neoplasm (PanIN) versus intraductal papillary mucinous neoplasm (IPMN) associated pancreatic adenocarcinoma. *J. Clin. Med.* **9**, 3102 (2020).
40. Middha, S. et al. Reliable pan-cancer microsatellite instability assessment by using targeted next-generation sequencing data. *JCO Precis. Oncol.* **2017**, PO.17.00084 (2017).
41. O'Connor, C. A. et al. Lynch syndrome and somatic mismatch repair variants in pancreas cancer. *JAMA Oncol.* **5**, e243651 (2024).
42. Noë, M. et al. Genomic characterization of malignant progression in neoplastic pancreatic cysts. *Nat. Commun.* **11**, 4085 (2020).
43. Skaro, M. et al. Prevalence of germline mutations associated with cancer risk in patients with intraductal papillary mucinous neoplasms. *Gastroenterology* **156**, 1905–1913 (2019).
44. Park, W. et al. Clinico-genomic characterization of *ATM* and HRD in pancreas cancer: application for practice. *Clin. Cancer Res.* **28**, 4782–4792 (2022).
45. Momtaz, P. et al. Pancreas cancer and BRCA: a critical subset of patients with improving therapeutic outcomes. *Cancer* **127**, 4393–4402 (2021).
46. Reiss, K. A. et al. Phase II study of maintenance rucaparib in patients with platinum-sensitive advanced pancreatic cancer and a pathogenic germline or somatic variant in *BRCA1*, *BRCA2*, or *PALB2*. *J. Clin. Oncol.* **39**, 2497–2505 (2021).
47. Buller, R. E. et al. The p53 mutational spectrum associated with BRCA1 mutant ovarian cancer1. *Clin. Cancer Res.* **7**, 831–838 (2001).
48. Ambrogio, C. et al. KRAS dimerization impacts MEK inhibitor sensitivity and oncogenic activity of mutant KRAS. *Cell* **172**, 857–868.e15 (2018).
49. Zhang, Z. et al. Wildtype Kras2 can inhibit lung carcinogenesis in mice. *Nat. Genet.* **29**, 25–33 (2001).
50. To, M. D. et al. Kras regulatory elements and exon 4A determine mutation specificity in lung cancer. *Nat. Genet.* **40**, 1240–1244 (2008).
51. Westcott, P. M. K. et al. The mutational landscapes of genetic and chemical models of Kras-driven lung cancer. *Nature* **517**, 489–492 (2015).
52. Hobbs, G. A. et al. Atypical KRASG12R mutant is impaired in PI3K signaling and macropinocytosis in pancreatic cancer. *Cancer Discov.* **10**, 104–123 (2020).
53. Yousef, A. et al. Impact of KRAS mutations and co-mutations on clinical outcomes in pancreatic ductal adenocarcinoma. *NPJ Precis. Oncol.* **8**, 27 (2024).
54. Conroy, T. et al. FOLFIRINOX or gemcitabine as adjuvant therapy for pancreatic cancer. *N. Engl. J. Med.* **379**, 2395–2406 (2018).
55. Stossel, C. et al. Spectrum of response to platinum and PARP inhibitors in germline *BRCA*–associated pancreatic cancer in the clinical and preclinical setting. *Cancer Discov.* **13**, 1826–1843 (2023).
56. Kindler, H. L. et al. Overall survival results from the POLO trial: a phase III study of active maintenance olaparib versus placebo for germline BRCA-mutated metastatic pancreatic cancer. *J. Clin. Oncol.* **40**, 3929–3939 (2022).
57. Hosein, A. N. et al. Loss of Rnf43 accelerates Kras-mediated neoplasia and remodels the tumor immune microenvironment in pancreatic adenocarcinoma. *Gastroenterology* **162**, 1303–1318. e18 (2022).
58. Lin, L. et al. The Hippo effector YAP promotes resistance to RAF- and MEK-targeted cancer therapies. *Nat. Genet.* **47**, 250–256 (2015).

59. Abboud, Y. et al. Increasing pancreatic cancer incidence in young women in the United States: a population-based time-trend analysis, 2001–2018. *Gastroenterology* **164**, 978–989. e6 (2023).
60. Arora, K. et al. Genetic ancestry correlates with somatic differences in a real-world clinical cancer sequencing cohort. *Cancer Discov.* **12**, 2552–2565 (2022).

[1]Department of Medicine, Memorial Sloan Kettering Cancer Center, New York City, NY, USA. [2]David M. Rubenstein Center for Pancreatic Cancer Research, Memorial Sloan Kettering Cancer Center, New York City, NY, USA. [3]Department of Pathology and Laboratory Medicine, Memorial Sloan Kettering Cancer Center, New York City, NY, USA. [4]Department of Epidemiology and Biostatistics, Memorial Sloan Kettering Cancer Center, New York City, NY, USA. [5]Marie-Josée and Henry R. Kravis Center for Molecular Oncology, Memorial Sloan Kettering Cancer Center, New York City, NY, USA. [6]Department of Surgery, Memorial Sloan Kettering Cancer Center, New York City, NY, USA. [7]Human Oncology and Pathogenesis Program, Memorial Sloan Kettering Cancer Center, New York City, NY, USA. [8]These authors contributed equally: Anna M. Varghese, Maria A. Perry. ✉e-mail: bandlamc@mskcc.org; oreillye@mskcc.org

Methods

The research was reviewed and overseen by the Institutional Review Board at Memorial Sloan Kettering Cancer Center.

Study cohort

Between January 2014 and September 2021, 2,671 tumor and matched normal DNA samples from 2,566 patients with PDAC were subjected to molecular testing using MSK-IMPACT, an FDA-authorized clinical next-generation sequencing panel. Patients provided consent for tumor profiling under an institutional Memorial Sloan Kettering Cancer Center (MSK) IRB-approved research prospective protocol, 'Tumor Genomic Profiling in Patients Evaluated for Targeted Cancer Therapy' (NCT01775072). Patients were not compensated financially for participation in the study. Tumor samples with low sequence coverage (<100×) or no detectable somatic alterations likely due to low tumor content quality were excluded (112 samples from 99 patients). Upon further review, 62 patients were excluded for having a diagnosis other than PDAC, and an additional 69 patients were excluded for having incomplete medical records. From the remaining 2,336 patients, one representative sample from each patient was selected for further analysis based on several criteria including higher tumor purity, higher sequence coverage, sample passing of allele-specific copy number (FACETS) quality control criteria (https://github.com/taylor-lab/facets-preview/) and the specific IMPACT panel size on which the specimen was sequenced. Of these 2,336 patients, 1,480 patients who had at least one year of clinical follow-up at our center between January 2014 and March 2021 underwent comprehensive clinical annotation after manual curation of medical health records. Genetic ancestry was inferred from IMPACT as described previously[60]. Comprehensive demographic and clinical information are included in Table 1. Self-reported sex information was collected from patient medical records. No sex-based criteria were used to select patients in this study. Gender information was not considered in the study.

Tumor sequencing and mutation assessment

Tumor samples were sequenced using the MSK-IMPACT targeted sequencing panel as described previously[33]. Briefly, tumor type and purity were assessed by pathology from H&E-stained slides of tumor samples. Genomic DNA from formalin-fixed, paraffin-embedded (FFPE) tumor and matched normal (peripheral blood) samples was extracted, and targeted sequencing was performed using custom DNA probes against all exons and selected introns of a given panel of cancer genes. Tumors were sequenced using four different generations of MSK-IMPACT panels containing 341 genes (n = 17 samples), 410 genes (n = 438), 468 genes (n = 1,536) and 505 genes (n = 345). The median sequencing depth of tumors was 606× (25th percentile: 469×, 75th percentile: 749×). The median purity of the tumors, estimated by FACETS, was 31%. For tumors without FACETS estimated purity, the pathologist estimated tumor purity was used to determine if the sample meets sufficient quality criteria to be included in the cohort (see above). Somatic mutations, copy number alterations and structural rearrangements in select genes were identified using a previously described pipeline validated for use in a Clinical Laboratory Improvement Amendments (CLIA)-compliant laboratory[33]. All somatic alterations were annotated for clinical actionability using OncoKB version. 4.12, December 2023[34]. All somatic alterations that were identified as 'oncogenic' or 'likely oncogenic' by OncoKB were considered as drivers and used exclusively in all analyses (annotated as $[Gene]^{MUT}$, regardless of alteration type) unless otherwise noted. Genes were included in the oncoprint in Fig. 1a if they met any of the following criteria: mutated in >5% of patients, MAPK pathway, MYC pathway, clinically actionable genes mutated in ≥1% of patients, or significantly enriched in either other-$MAPK^{MUT}$ or $MAPK^{WT}$ tumors. Pathway gene lists were defined by the oncogenic signaling pathways described in ref. 61. Germline variant discovery and pathogenicity assessment was performed as previously described[62,63]. MSI was determined by MSIsensor, with tumors identified with an MSIsensor score of 10 or higher classified as microsatellite instable (MSI-H, microsatellite instability high)[64,65]. A select subset of the cohort (n = 90 patients) received additional clinical testing for fusions using the custom RNA-seq panel (MSK-Fusion) that utilizes Archer Multiplex PCR technology[66]. All tumors wild-type for *KRAS* mutations were evaluated for read evidence at subdetection thresholds. In these tumors, we genotyped known *KRAS* hotspot mutations using a custom tool (https://github.com/mskcc/GetBaseCounts-MultiSample) and identified reads with mapping quality scores of at least 20. All mapping reads were manually reviewed using IGV (http://software.broadinstitute.org/software/igv/) to identify high-quality reads. A read is considered high quality if there are no mismatches and if the evidence supporting the mutated base is not in the leading or trailing ten bases of the sequencing read.

RNA sequencing for fusion detection

We performed RNA sequencing on 11 tumor specimens derived from FFPE tissue blocks. Fusions were called using FusionCatcher v1.20 (https://github.com/ndaniel/fusioncatcher) and Arriba v2.1.0 (https://github.com/suhrig/arriba). Results from each caller were merged into a single output file according to matching gene IDs and breakpoints. Noncoding fusions from FusionCatcher were excluded from the final output of the pipeline. All fusion calls were annotated by OncoKB. Two tumors harbored activating fusions involving MAPK pathway genes. In one sample, the *ATP1B1–NRG1* rearrangement fused the third exon of *ATP1B1* to the second exon of *NRG1*. In another sample, the fourteenth exon of *GIT2* was fused to the fourth exon of *BRAF*. In both events, the entire kinase domain of the 3′ gene was retained.

Allele-specific copy number analysis

Allele-specific copy number was inferred using the FACETS algorithm (v0.5.14)[67]. Briefly, FACETS was run on each tumor sample in a two-step mode as previously described[28]. The first step aims to identify the normalized tumor to normal sequencing coverage ratio corresponding to the diploid state. Using this, the second step aims to identify the focal gains and losses. FACETS-derived purity and ploidy estimate for the tumor sample and the allele-specific integer copy number for each locus was inferred. To identify and exclude tumors with poor quality copy number fits, we applied a series of quality control criteria (https://github.com/taylor-lab/facets-preview/) that include degree of evidence supporting the diploid state, the fraction of the genome with homozygous deletions, fraction of the genome that is estimated to be subclonal, hypersegmentation, concordance between integer copy number estimate and the allelic configuration and whether FACETS was able to estimate purity (C.B., D.M., Ino de Bruijn, Mingxuan Zhang, Michael V. Gormally et al., in revision). Overall, 1,555 of 2,322 tumor samples for which we were able to generate FACETS profiles had sufficiently high-quality copy number fits evaluable for further analysis. WGD status is inferred as previously described (https://github.com/mskcc/facets-suite)[30]. Briefly, a tumor is deemed to have undergone genome doubling if more than 50% of the autosomal genome has a major copy number of 2 or higher. In our cohort, 339 of 1,555 tumors were WGD-positive. Clonality of somatic mutations was determined as described previously[68]. Briefly, we first infer the cancer cell fraction (CCF) of mutation using the variant allele frequency of the somatic mutation, the integer copy number at the locus, the read coverage and the FACETS estimated tumor purity. A mutation is deemed to be clonal if either the CCF estimate is 80% or higher, or if the CCF estimate is 70% or higher and the upper bound of the 95th percentile CI of the CCF estimate is greater than 90% (https://github.com/mskcc/facets-suite). LOH at specific loci harboring germline/somatic mutations or WT alleles was assessed using allele-specific copy number inference from FACETS. A locus is considered to have LOH if the *lcn* is 0.

KRAS allelic imbalance and mutant allele dosage gains

Of the 1,555 tumors with sufficiently high-quality copy number profiles, 1,157 were $KRAS^{MUT}$ with determinable integer copy number. We then assigned each of these tumors to six different allelic copy number states based on the total copy number (*tcn*) and lower copy number (*lcn*) at the *KRAS* locus as well as the WGD status (Fig. 3a). In non-WGD tumors, diploid tumors with *tcn*:*lcn* of 2:1 were considered as 'Balanced' (heterozygous). Tumors with complete loss of one inherited allele (lcn of 0) were considered as 'LOH' if the *tcn* is 1, and 'CNLOH' if *tcn* is >1. Tumors were considered to harbor *KRAS* 'amplifications' if our clinical pipeline identified focal *KRAS* amplifications or the *tcn* in FACETS was ≥5 in the absence of WGD, or ≥6 with WGD. The tumors that retained both inherited maternal and paternal alleles but have gained additional copies of one or both inherited alleles were considered as 'Gains'. Among WGD-positive tumors, we accounted for the higher balanced state (*tcn*:*lcn* of 4:2) in ascribing allelic copy number states associated with losses and gains. WGD-positive tumors that acquired single-copy losses (irrespective of whether the loss targeted the WT or the mutant allele) were considered as 'Loss after WGD'. To be considered as a 'Gain' in WGD-positive tumors, the *tcn* is required to be 5 or higher.

The expected number of *KRAS* mutant alleles is estimated using the observed variant allele frequency, tumor purity and total copy number at the *KRAS* locus as previously described[28,69]. We considered tumors with a higher number of mutant copies than WT copies to have undergone mutant allele selection. These include tumors identified as having 'LOH' (*tcn*:*lcn* of 1:0 for non-WGD tumors and 2:0 for WGD-positive tumors), 'CNLOH' (complete loss of wild-type with either ≥2 mutant copies in non-WGD tumors, or, ≥3 mutant copies in WGD-positive tumors), 'Gain of mutant' (with higher number of mutant copies than wild-type copies), and finally, among WGD-positive tumors, 'WGD+Loss of WT' tumors in which a copy number losses after WGD event targeted the wild-type allele (Fig. 3c). Tumors in which selection following copy number gains/losses resulted in preferential retention of the *KRAS* WT allele were rare ($n = 32$, 'WT selection', Fig. 3c) and were not considered further.

Statistics and reproducibility

Enrichment testing was performed using two-sided Fisher's exact tests with multiple test correction by the FDR method where appropriate. For gene-level enrichment analyses, we evaluated all cancer genes that are captured on all versions of the MSK-IMPACT panels ($n = 341$ genes) and were altered in at least 3 samples in the dataset. Unless otherwise noted, enrichment tests were limited to alterations detected by MSK-IMPACT and annotated as drivers (oncogenic or likely oncogenic) by OncoKB. Error bars on all figures showing counts/prevalence data represent 95% CIs of the binomial probability. Two-sided chi-squared tests were used for testing differences in prevalence of nonbinary variables such as ancestry and clinical stage. Two-sided Wilcoxon rank sum tests were used for comparison of numeric variables such as age. In boxplots, the center line represents the median, lower and upper hinges show the 25th and 75th percentiles, and lower and upper whiskers show the minimum and maximum values no further than 1.5× the interquartile range, respectively, with outlier points beyond this range plotted individually. Analyses were conducted using R version 4.3.0 with the rstatix (v0.7.2), stats (v4.3.0) and binom (v1.1.1.1) packages and visualized using ggplot2 (v3.4.4). Oncoprints were generated using cBioPortal for Cancer Genomics[70–72].

Survival

OS was calculated as the interval from date of IMPACT sample collection to date of death or last follow-up. Patients with no follow-up after IMPACT sample collection were censored on day 1 ($n = 9$). Patients with missing date of IMPACT specimen collection ($n = 2$) or those with IMPACT specimen collection before January 2014 ($n = 64$) were excluded from survival analyses. All *P* values and adjusted HRs associated with survival analyses are from multivariable Cox proportional hazards models accounting for covariates including age, sex, ancestry and interval from diagnosis to sample collection. Full models are shown in Extended Data Tables. Covariates were selected based on statistically significant univariate associations with OS. MSI type and TMB were not found to have a statistically significant association with OS in a univariate model and therefore were not included as covariates in multivariable models. Models were either stratified by clinical stage at diagnosis or evaluated within each stage to account for known differences in OS by stage. Median OS values were calculated using the univariate Kaplan–Meier estimator. Analyses were conducted using R version 4.3.0 with the tidyverse (v2.0.0), survival (v3.5-5) and gtsummary (v1.7.2) packages.

For stage and survival analyses associated with *KRAS* copy number (Fig. 3), resectable patients who had experienced a recurrence by the time of sample collection were excluded ($n = 95$) to limit variation in disease progression within the stage. For OS comparison by binary gene alteration status (Fig. 5d), genes were considered if they had a somatic alteration prevalence of at least 3% of metastatic patients who had received standard-of-care chemotherapy with either 5-FU to gemcitabine backbones who could be evaluated for OS ($n = 473$ patients, 13 genes). Samples were then limited to those with high purity (30% or higher) to reduce the bias of false negatives in the WT group ($n = 304$ patients). Chemotherapy backbone (5-FU versus gemcitabine/nab-paclitaxel) was not significantly associated with OS and was therefore not included as a covariate ($P > 0.05$). Multivariable Cox proportional hazards models were constructed for each gene (Extended Data Table 5), and *P* values of the genomic alterations in each model were adjusted by FDR with $n = 13$.

Reporting summary

Further information on research design is available in the Nature Portfolio Reporting Summary linked to this article.

Data availability

Genomic and associated clinical data for all patients and tumor samples included in this study have been deposited in cBioPortal for Cancer Genomics and are publicly accessible and downloadable at https://www.cbioportal.org/study/summary?id=pdac_msk_2024. Raw tumor and normal sequencing data from MSK-IMPACT, as well as all data associated with germline variants, are considered protected information and access is available under restricted access subject to additional institutional approvals. These data may be requested for appropriate use from the corresponding authors by email (bandlamc@mskcc.org, oreillye@mskcc.org); requests will be reviewed within 4 weeks. Data will be shared for a span of 2 years within 2 weeks of execution of a data transfer agreement with MSK, which will retain all title and rights to the data and results from their use.

Code availability

Algorithms and R packages used are open-source and described in the Methods. The FACETS algorithm for allele-specific copy number is available on GitHub at https://github.com/taylor-lab/facets-preview/. The OncoKB knowledge base used for annotation is available at https://www.oncokb.org/ and through the API on GitHub at https://github.com/oncokb/oncokb-annotator.

References

61. Sanchez-Vega, F. et al. Oncogenic signaling pathways in The Cancer Genome Atlas. *Cell* **173**, 321–337.e10 (2018).
62. Cheng, D. T. et al. Comprehensive detection of germline variants by MSK-IMPACT, a clinical diagnostic platform for solid tumor molecular oncology and concurrent cancer predisposition testing. *BMC Med. Genomics* **10**, 33 (2017).

63. Srinivasan, P. et al. The context-specific role of germline pathogenicity in tumorigenesis. *Nat. Genet.* **53**, 1577–1585 (2021).
64. Niu, B. et al. MSIsensor: microsatellite instability detection using paired tumor-normal sequence data. *Bioinformatics* **30**, 1015–1016 (2014).
65. Hu, Z. I. et al. Evaluating mismatch repair deficiency in pancreatic adenocarcinoma: challenges and recommendations. *Clin. Cancer Res.* **24**, 1326–1336 (2018).
66. Benayed, R. et al. High yield of RNA sequencing for targetable kinase fusions in lung adenocarcinomas with no mitogenic driver alteration detected by DNA sequencing and low tumor mutation burden. *Clin. Cancer Res.* **25**, 4712–4722 (2019).
67. Shen, R. & Seshan, V. E. FACETS: allele-specific copy number and clonal heterogeneity analysis tool for high-throughput DNA sequencing. *Nucleic Acids Res.* **44**, e131 (2016).
68. Jonsson, P. et al. Tumour lineage shapes BRCA-mediated phenotypes. *Nature* **571**, 576–579 (2019).
69. Dentro, S. C., Wedge, D. C. & Van Loo, P. Principles of reconstructing the subclonal architecture of cancers. *Cold Spring Harb. Perspect. Med.* **7**, a026625 (2017).
70. Cerami, E. et al. The cBio Cancer Genomics Portal: an open platform for exploring multidimensional cancer genomics data. *Cancer Discov.* **2**, 401–404 (2012).
71. Gao, J. et al. Integrative analysis of complex cancer genomics and clinical profiles using the cBioPortal. *Sci. Signal* **6**, pl1 (2013).
72. De Bruijn, I. et al. Analysis and visualization of longitudinal genomic and clinical data from the AACR Project GENIE Biopharma Collaborative in cBioPortal. *Cancer Res.* **83**, 3861–3867 (2023).

Acknowledgements

This work was supported by NIH/NCI P30CA008748 to MSK (to A.M.V., M.A.P., J.F.C., S.N., D. Muldoon, A.E., A.Z., C.F., M.M., B.N., O.B., F.B., D.P.K., A.R.B., D. Mandelker, E.V., W.P., K.H.Y., Z.K.S., M.A.S., W.R.J., A.C.W., D.C., M.C., N.S., M.F.B., C.A.I.-D., C.B., E.M.O.), R01 CA227534 (to M.F.B.), P50CA257881 (to E.M.O., O.B., W.P., A.C.W., M.C. and C.A.I.-D.), Break Through Cancer (to E.M.O., W.P. and C.A.I.-D.) and Parker Institute for Cancer Immunotherapy (to E.M.O. and W.P.). We acknowledge the David M. Rubenstein Center for Pancreatic Cancer Research, the Marie-Josée and Henry R. Kravis Center for Molecular Oncology and the Molecular Diagnostics Service at MSK. We also thank the patients who were included in this study along with their families. The funders had no role in study design, data collection and analysis, decision to publish or preparation of the manuscript.

Author contributions

A.M.V., M.A.P., N.S., M.F.B., C.A.I.-D., C.B. and E.M.O. conceived the study. A.M.V, M.A.P., J.F.C., S.N., D. Muldoon, D.C., M.C., N.S., M.F.B., C.B. and E.M.O. designed and performed data analysis. J.F.C. and M.C. provided statistical expertise and analyzed clinical outcomes data. M.M., D. Mandelker and Z.K.S. provided germline variant pathogenicity assessment. A.E. provided project management. A.Z., C.F., B.N., A.R.B, D. Mandelker, E.V., Z.K.S. and M.F.B. assisted with prospective genomic and clinical data collection and sample annotation. Z.K.S., N.S. and M.F.B. supported consent infrastructure. O.B. and E.V. assisted with sample acquisition for additional analysis. A.M.V., F.B., D.P.K., W.P., K.H.Y., M.A.S., W.R.J, A.C.W. and E.M.O. provided samples. A.M.V., M.A.P., C.B. and E.M.O. wrote the manuscript with input from all authors. All authors reviewed and approved the manuscript. C.B. and E.M.O. contributed equally as senior authors.

Competing interests

M.A.P. declares stock ownership in Amgen. A.M.V. declares consulting activity from AstraZeneca (spouse), Eli Lilly (spouse) and Paige AI (spouse), and intellectual property rights (SOPHiA Genetics) (spouse). B.N. is a current employee of Eli Lilly and Company. D. Mandelker declares consulting fees from AstraZeneca. F.B. receives research support from BMS. D.P.K. receives funding from the Thompson Family Foundation and Applebaum Foundation and is a consultant at Merck, BMS, BeiGene, Lilly, Abbvie, Incyte, Janssen, Listen and TG Therapeutics. A.R.B. declares stock ownership in Johnson & Johnson and intellectual property rights in SOPHiA Genetics. W.P. receives research funding from Merck, Astellas, Miracogen, Amgen and Revolution Medicines, is a consultancy/advisory board member for Astellas, EXACT Therapeutics, Innovent Biologics and Regeneron and has received honoraria for CME: American Physician Institute, Integrity. M.F.B. declares consulting activity from AstraZeneca, Eli Lilly and Paige AI and intellectual property rights (SOPHiA Genetics). E.M.O. receives research funding from Agenus, Amgen, Genentech/Roche, BioNTech, AstraZeneca, Arcus, Elicio, Parker Institute, NIH/NCI and Digestive Care, consulting/DSMB role at Arcus, Ability Pharma, Alligator, Agenus, BioNTech, Ipsen, Merck, Moma Therapeutics, Novartis, Syros, Leap Therapeutics, Astellas, BMS, Fibrogen, Revolution Medicine, Merus, Moma Therapeutics and Tango; Agios (spouse), Genentech-Roche (spouse), Eisai (spouse) Servier (spouse). The remaining authors declare no competing interests.

Additional information

Extended data is available for this paper at https://doi.org/10.1038/s41591-024-03362-3.

Supplementary information The online version contains supplementary material available at https://doi.org/10.1038/s41591-024-03362-3.

Correspondence and requests for materials should be addressed to Chaitanya Bandlamudi or Eileen M. O'Reilly.

Peer review information *Nature Medicine* thanks Mariano Ponz-Sarvise, Channing Der and the other, anonymous, reviewer(s) for their contribution to the peer review of this work. Primary Handling Editor: Anna Maria Ranzoni, in collaboration with the *Nature Medicine* team.

https://doi.org/10.1038/s41591-024-03362-3

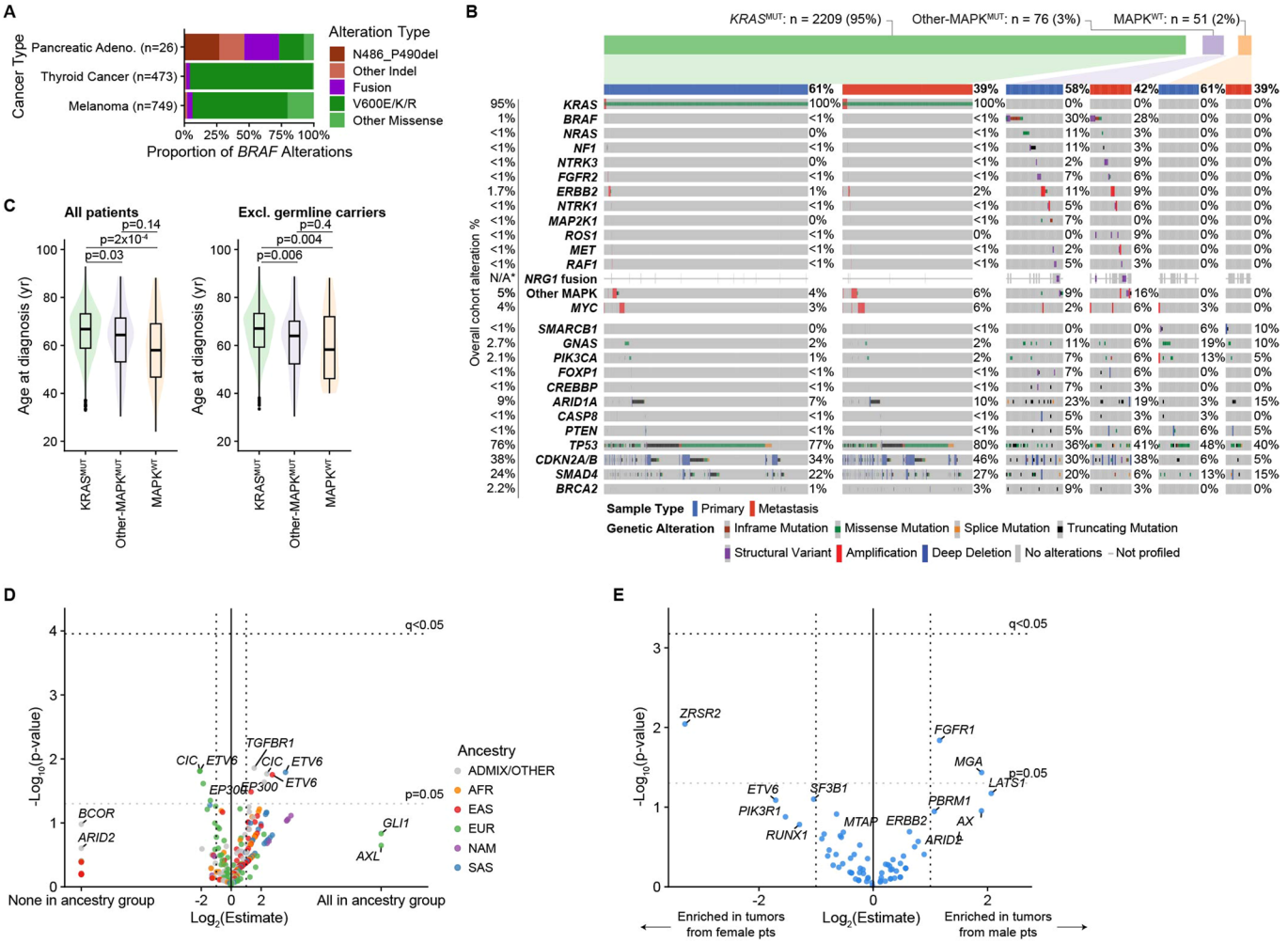

Extended Data Fig. 1 | Somatic alteration landscape in PDAC: additional insights. a, Prevalence of *BRAF* alteration types in PDAC, melanoma and thyroid cancer. **b**, Oncoprint of somatic oncogenic alterations with tumor samples grouped by genomic subtype (as in Fig. 1a) and by primary or metastasis sample type. **c**, Age at diagnosis across genomic groups including all patients (left, $n = 2{,}336$) and excluding patients with pathogenic germline variants (right, $n = 2{,}006$). Nominal *P* values indicate statistical comparison by two-sided Wilcoxon rank sum test. Boxes represent the 25th, 50th (median) and 75th percentiles. Whiskers represent the minimum and maximum values, no further than 1.5× the interquartile range (IQR) from the respective upper and lower quartiles, with points beyond this range plotted individually. **d**, Gene-level alteration enrichment by genetic ancestry ($n = 75$ genes with sufficient sample size). **e**, Gene-level alteration enrichment by sex ($n = 75$ genes with sufficient sample size). Enrichment was calculated using a two-sided Fisher exact test with *P* values adjusted for multiple testing by FDR for assessment of significance for **d** and **e**.

https://doi.org/10.1038/s41591-024-03362-3

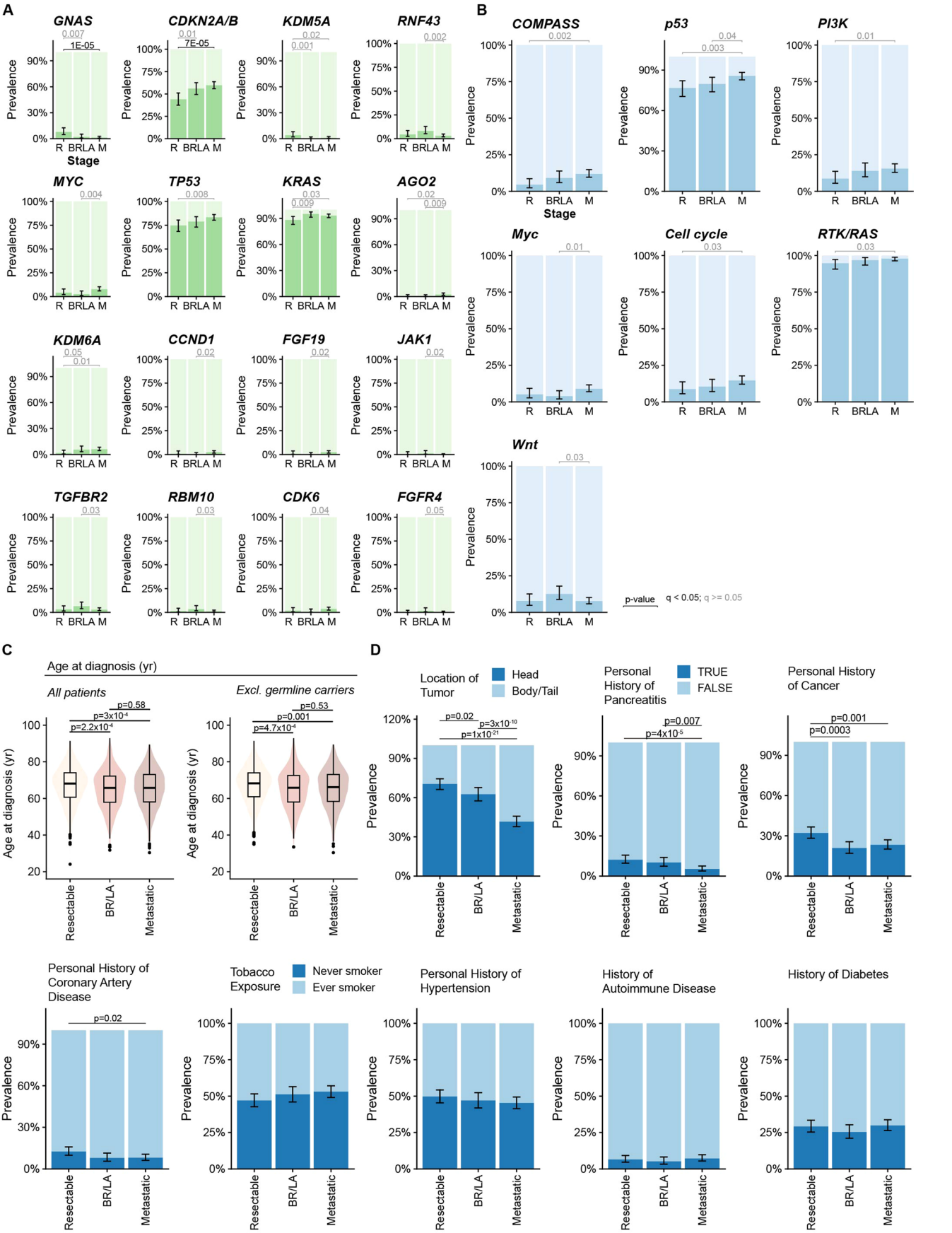

Extended Data Fig. 2 | See next page for caption.

https://doi.org/10.1038/s41591-024-03362-3

Extended Data Fig. 2 | Stage differences in pathway and gene alteration patterns, age and additional clinical features. a,**b**, Pathway- (**a**) and gene-level alteration (**b**) prevalence by clinical stage at diagnosis. Analysis limited to high-purity tumor samples (n = 1,076) and genes or pathways altered in at least 3 tumors in at least one stage. **c**, Age at diagnosis across the clinical stages at diagnosis including all patients (left, n = 2,336) and excluding patients with pathogenic germline variants (right, n = 2,006). Boxes represent the 25th, 50th (median) and 75th percentiles. Whiskers represent the minimum and maximum values, no further than 1.5× the interquartile range (IQR) from the respective upper and lower quartiles, with points beyond this range plotted individually. Groups were compared using two-sided Wilcoxon rank sum tests; nominal P value displayed. **d**, Tumor location, tobacco exposure and personal history of pancreatitis, hypertension, cancer, autoimmune disease, coronary artery disease and diabetes by clinical stage at diagnosis (n = 1,480). Error bars represent 95th percentile binomial CIs around the mean for **a**, **b** and **d**. Enrichment was calculated using a two-sided Fisher exact test for **a**, **b** and **d** with nominal P values displayed. P values were adjusted for multiple testing by FDR for assessment of significance for **a** and **b** (colored by $P_{adj} < 0.05$).

https://doi.org/10.1038/s41591-024-03362-3

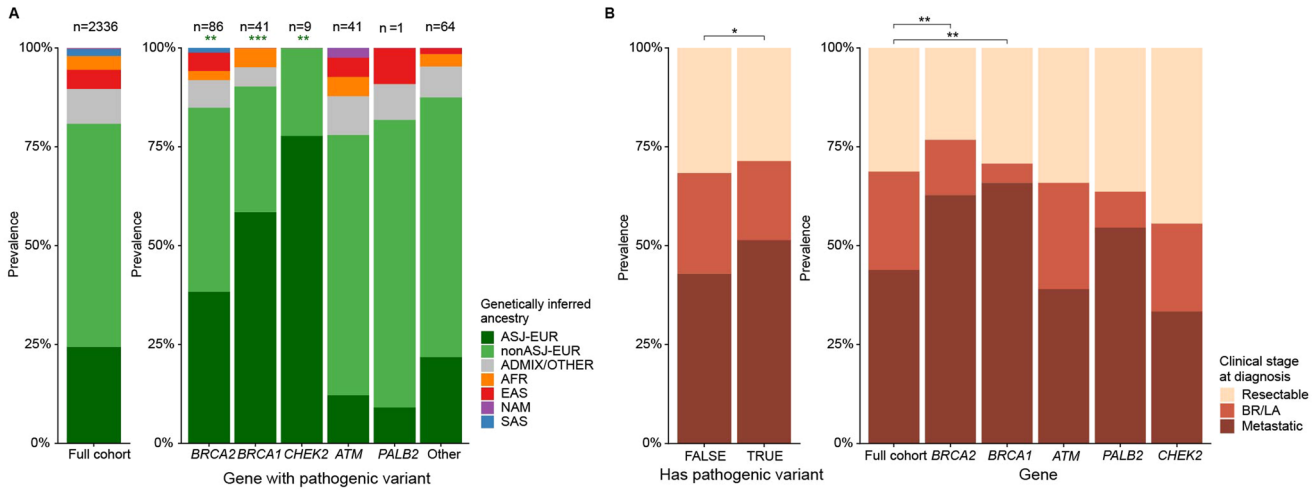

Extended Data Fig. 3 | Pathogenic germline variant prevalence by ancestry and stage. a, Distribution of genetically inferred ancestry across the overall cohort (left) and by germline mutated genes. Asterisks denote enrichment of ASJ-EUR ancestry by Fisher's exact test ($q < 0.05$). **b**, Distribution of clinical stage at diagnosis across the overall cohort (left) and by germline mutated genes. Asterisks denote chi-squared test ($q < 0.05$).

https://doi.org/10.1038/s41591-024-03362-3

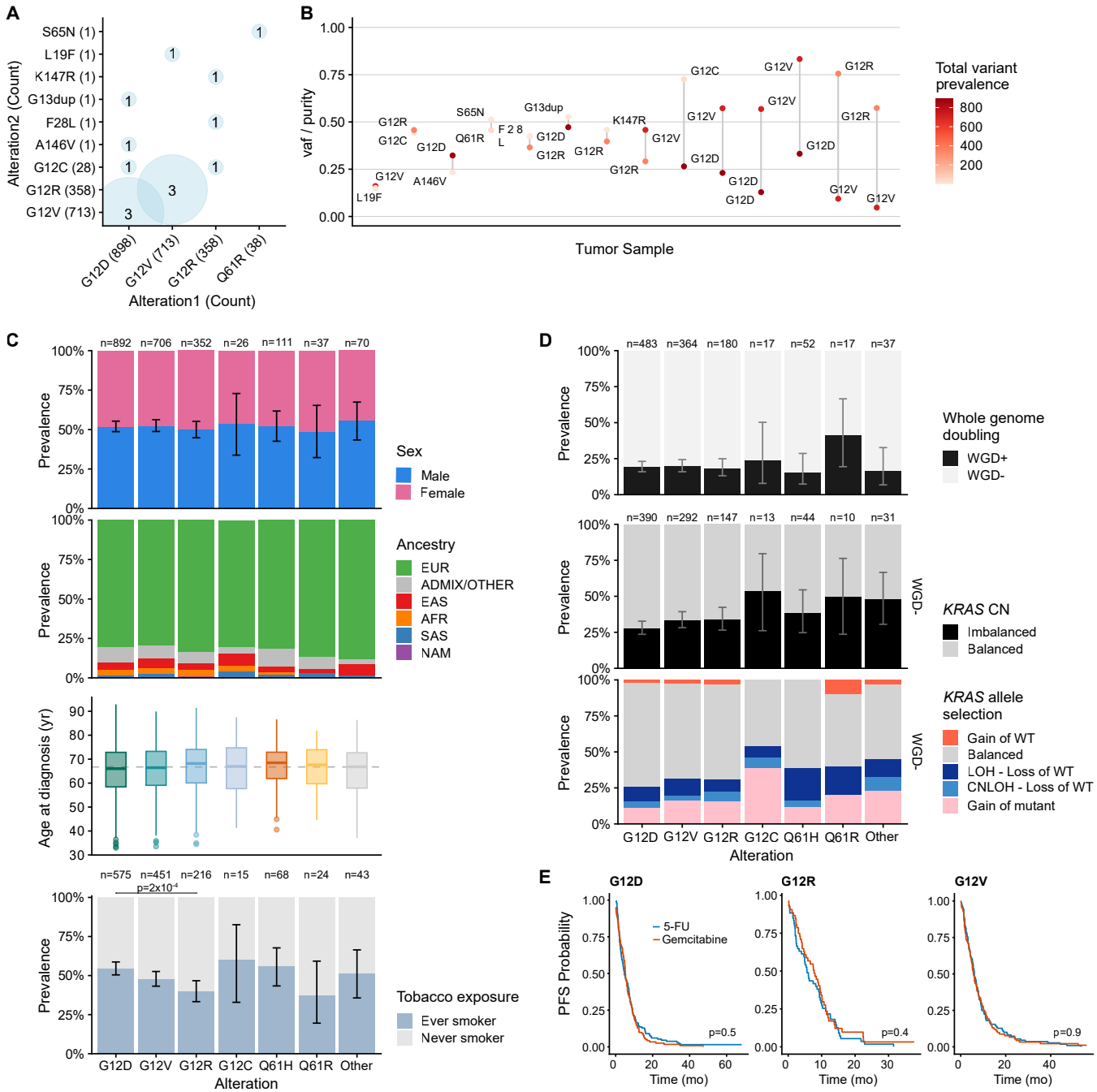

F

	G12D				G12R				G12V			
	N	HR[1]	95% CI[1]	p-value	N	HR[1]	95% CI[1]	p-value	N	HR[1]	95% CI[1]	p-value
Chemotherapy												
5-FU	172	—	—		60	—	—		134	—	—	
Gemcitabine	176	1.05	0.83, 1.32	0.7	53	0.83	0.55, 1.26	0.4	124	1.01	0.77, 1.33	>0.9
Sex												
Female	164	—	—		61	—	—		118	—	—	
Male	184	0.90	0.72, 1.12	0.3	52	0.88	0.56, 1.38	0.6	140	1.01	0.78, 1.31	>0.9
Age at dx	348	1.00	1.00, 1.00	0.5	113	1.00	1.00, 1.00	0.6	258	1.00	1.00, 1.00	0.8
Ancestry												
EUR	286	—	—		95	—	—		203	—	—	
non -EUR	62	1.14	0.85, 1.54	0.4	18	1.13	0.63, 2.02	0.7	55	1.38	1.01, 1.88	**0.044**

[1]HR = Hazard Ratio, CI = Confidence Interval

Extended Data Fig. 4 | See next page for caption.

https://doi.org/10.1038/s41591-024-03362-3

Extended Data Fig. 4 | Differential genomic and prognostic features of KRAS variants: additional insights. a, Bubble chart of co-occurring *KRAS* mutations. Number and bubble size indicate the prevalence of a given combination, and number in parentheses is the prevalence of the mutation in the overall cohort. **b**, Purity-adjusted variant allele frequency (VAF) of *KRAS* mutations by tumor, ordered by difference in VAF. Please note the 14 tumors shown here are excluded from Fig. 4. **c**, Prevalence of sex, genetic ancestry, age at diagnosis and smoking status by *KRAS* variant. Dotted line for age shows overall median. *P* value denotes two-sided Fisher's exact test. Boxes for age represent the 25th, 50th (median) and 75th percentiles. Whiskers represent the minimum and maximum values, no further than 1.5× the interquartile range (IQR) from the respective upper and lower quartiles, with points beyond this range plotted individually. **d**, Prevalence of WGD by *KRAS* variant ($n = 1{,}150$); prevalence of *KRAS* allelic imbalance and *KRAS* allele selection state by *KRAS* variant among diploid tumors ($n = 927$). **e**,**f**, Progression-free survival (PFS) differences between first-line standard-of-care treatments across the different *KRAS* variant groups. **e**, Kaplan–Meier curves for PFS differences between FOLFIRINOX (5-FU) and gemcitabine for *KRAS* G12D, G12V and G12R. *P* values represent statistical comparison of univariate Kaplan–Meier curves by log-rank test. **f**, Multivariable Cox proportional hazards model for **e**. *P* values are nominal two-sided *P* values from the Cox regression model. Error bars represent 95th percentile binomial CIs around the mean for **c** and **d**.

https://doi.org/10.1038/s41591-024-03362-3

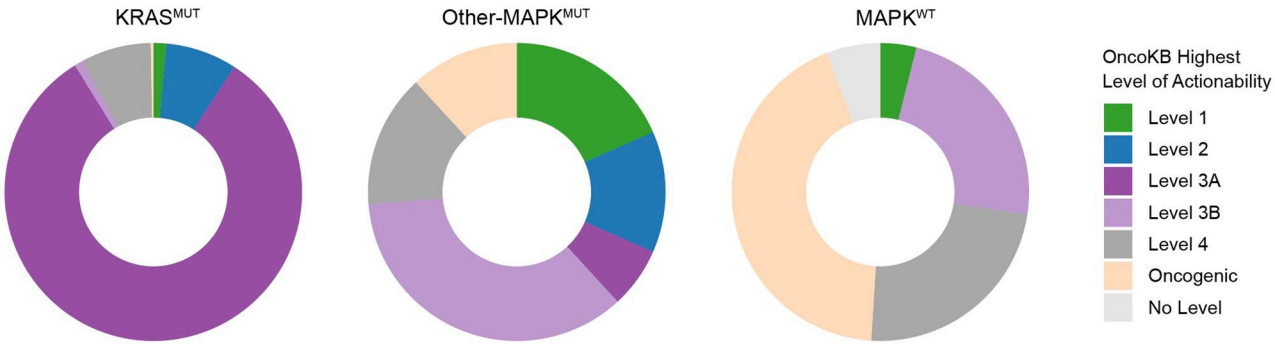

Extended Data Fig. 5 | OncoKB clinical actionability across the three genomic subtypes of PDAC. Prevalence of actionable alterations by OncoKB levels of actionability across *KRAS*^{MUT}, other-*MAPK*^{MUT} and *MAPK*^{WT} tumors.

https://doi.org/10.1038/s41591-024-03362-3

Extended Data Table 1 | Overall survival by genomic group

	All			*Excl. targeted treatment*		
Characteristic	**HR[1]**	**95% CI[1]**	**p-value**	**HR[1]**	**95% CI[1]**	**p-value**
Genomic group						
KRAS-alt	—	—		—	—	
Other-MAPK-alt	0.69	0.51, 0.93	**0.014**	0.95	0.70, 1.29	0.73
MAPK-WT	0.69	0.48, 0.98	**0.041**	0.68	0.47, 0.97	**0.035**
Sex						
Male	—	—		—	—	
Female	0.82	0.74, 0.91	**1.2e-04**	0.82	0.74, 0.91	**2.4e-04**
Age at dx	1.01	1.00, 1.01	**0.015**	1.01	1.00, 1.01	**0.039**
Ancestry						
EUR	—	—		—	—	
ADMIX/OTHER	1.06	0.89, 1.27	0.51	1.04	0.87, 1.24	0.68
EAS	1.02	0.80, 1.31	0.85	1.04	0.81, 1.34	0.73
AFR	1.19	0.91, 1.55	0.20	1.14	0.88, 1.49	0.32
SAS	1.50	1.04, 2.16	**0.032**	1.37	0.95, 1.99	0.093
Time from dx to collection (yr)	1.06	1.01, 1.11	**0.028**	1.07	1.02, 1.13	**0.011**
Disease status						
Primary	—	—		—	—	
Metastatic	1.52	1.18, 1.95	**0.001**	1.45	1.12, 1.88	**0.005**
Resection						
FALSE	—	—		—	—	
TRUE	0.60	0.46, 0.78	**1.8e-04**	0.56	0.43, 0.74	**4.9e-05**

[1]HR = Hazard Ratio, CI = Confidence Interval

OS by genomic group among all patients in the cohort considered for survival analysis (Methods, *n*=2,270; left), and among patients who did not receive targeted treatment for actionable alterations (*n*=2,187, right). Multivariable Cox proportional hazards model of OS, stratified by stage at diagnosis. Displayed *P* values are nominal two-sided *P* values associated with the observed hazard ratios from the multivariable regression models. HR, hazard ratio; CI, confidence interval. Bold numbers indicate *P* values <0.05.

https://doi.org/10.1038/s41591-024-03362-3

Extended Data Table 2 | Overall survival by *KRAS* mutant allele dosage

	Stratified			*Resectable*			*BR/LA*			*Metastatic*		
Characteristic	**HR[1]**	**95% CI[1]**	**p-value**	**HR[1]**	**95% CI[1]**	**p-value**	**HR[1]**	**95% CI[1]**	**p-value**	**HR[1]**	**95% CI[1]**	**p-value**
KRAS mutant allele CN			**3.5e-07**			**0.045**			**0.030**			**8.3e-05**
1	—	—		—	—		—	—		—	—	
2+	1.67	1.37, 2.03	**3.5e-07**	2.16	1.08, 4.33	**0.030**	1.67	1.07, 2.59	**0.023**	1.63	1.29, 2.07	**4.9e-05**
Sex			0.084			0.43			0.63			0.13
Male	—	—		—	—		—	—		—	—	
Female	0.87	0.74, 1.02	0.084	0.85	0.57, 1.27	0.43	0.93	0.68, 1.27	0.63	0.85	0.68, 1.05	0.14
Age at dx	1.01	1.00, 1.01	0.16	1.0	0.98, 1.01	0.60	1.02	1.01, 1.04	**0.003**	1.00	0.99, 1.01	0.89
Ancestry			**0.021**			0.92			0.54			**0.050**
EUR	—	—		—	—		—	—		—	—	
ADMIX/OTHER	0.93	0.71, 1.23	0.62	0.67	0.27, 1.67	0.39	1.12	0.69, 1.82	0.66	0.91	0.63, 1.30	0.59
EAS	1.24	0.87, 1.78	0.24	1.01	0.42, 2.42	0.98	1.11	0.58, 2.15	0.75	1.06	0.61, 1.84	0.85
AFR	1.23	0.82, 1.83	0.31	1.23	0.17, 8.96	0.84	1.80	0.95, 3.42	0.073	1.05	0.61, 1.79	0.87
SAS	2.78	1.43, 5.42	**0.003**	0.88	0.12, 6.46	0.90	1.67	0.23, 12.1	0.61	4.15	1.93, 8.91	**2.6e-04**
Time from dx to collection (yr)	1.17	1.08, 1.28	**2.4e-04**	3.69	2.00, 6.79	**6.0e-04**	1.12	1.01, 1.25	0.057	1.39	1.15, 1.69	**0.003**

[1]HR = Hazard Ratio, CI = Confidence Interval

OS by *KRAS* mutant allele dosage among patients with $KRAS^{MUT}$ tumors evaluable for *KRAS* allele-specific copy number considered for survival analysis (Methods, $n=865$). Multivariable Cox proportional hazards model of OS, stratified by stage at diagnosis and within each stage. Displayed *P* values are nominal two-sided *P* values associated with the observed hazard ratios from the multivariable regression models. Bold numbers indicate *P* values <0.05.

https://doi.org/10.1038/s41591-024-03362-3

Extended Data Table 3 | OS by *KRAS* copy number state

	Stratified			*Stratified (ref: Gain)*			*Resectable*			*BR/LA*			*Metastatic*		
Characteristic	**HR[1]**	**95% CI[1]**	**p-value**	**HR[1]**	**95% CI[1]**	**p-value**	**HR[1]**	**95% CI[1]**	**p-value**	**HR[1]**	**95% CI[1]**	**p-value**	**HR[1]**	**95% CI[1]**	**p-value**
KRAS CN state			**1.5e-07**			**1.5e-07**			**0.036**			0.071			**2.9e-05**
Balanced	—	—		0.65	0.53, 0.82	**1.7e-04**	—	—		—	—		—	—	
LOH	0.97	0.75, 1.25	0.80	0.63	0.47, 0.86	**0.004**	1.64	0.98, 2.77	0.062	0.68	0.41, 1.14	0.14	0.98	0.68, 1.43	0.93
Gain	1.53	1.22, 1.90	**1.7e-04**	—	—		2.44	1.14, 5.22	**0.021**	1.59	0.98, 2.57	0.061	1.44	1.10, 1.88	**0.008**
CNLOH	2.50	1.73, 3.63	**1.3e-06**	1.64	1.10, 2.45	**0.016**	3.89	0.93, 16.3	0.063	1.56	0.61, 3.98	0.35	2.95	1.91, 4.54	**9.1e-07**
Sex			0.074			0.074			0.39			0.61			0.17
Male	—	—		—	—		—	—		—	—		—	—	
Female	0.86	0.74, 1.01	0.074	0.86	0.74, 1.01	0.074	0.84	0.56, 1.25	0.39	0.92	0.67, 1.27	0.61	0.86	0.69, 1.07	0.17
Age at dx	1.01	1.00, 1.01	0.14	1.01	1.00, 1.01	0.14	1.0	0.98, 1.01	0.59	1.02	1.01, 1.04	**0.003**	1.00	0.99, 1.01	0.92
Ancestry			**0.015**			**0.015**			0.93			0.64			**0.043**
EUR	—	—		—	—		—	—		—	—		—	—	
ADMIX/OTHER	0.95	0.72, 1.25	0.72	0.95	0.72, 1.25	0.72	0.68	0.27, 1.70	0.41	1.08	0.66, 1.77	0.76	0.92	0.64, 1.32	0.64
EAS	1.28	0.90, 1.84	0.17	1.28	0.90, 1.84	0.17	0.95	0.40, 2.26	0.91	1.04	0.54, 2.02	0.90	1.10	0.63, 1.91	0.75
AFR	1.27	0.85, 1.90	0.24	1.27	0.85, 1.90	0.24	1.35	0.18, 9.89	0.77	1.72	0.90, 3.30	0.10	1.09	0.64, 1.87	0.75
SAS	2.81	1.44, 5.48	**0.002**	2.81	1.44, 5.48	**0.002**	0.97	0.13, 7.14	0.98	1.57	0.22, 11.4	0.66	4.28	1.99, 9.20	**2.0e-04**
Time from dx to collection (yr)	1.17	1.08, 1.28	**2.9e-04**	1.17	1.08, 1.28	**2.9e-04**	3.83	2.06, 7.14	**4.7e-04**	1.13	1.02, 1.26	**0.037**	1.39	1.15, 1.69	**0.003**

[1]HR = Hazard Ratio, CI = Confidence Interval

OS by *KRAS* copy number state among patients with $KRAS^{MUT}$ tumors and determinate *KRAS* allele-specific copy number considered for survival analysis (n=865). Multivariable Cox proportional hazards model of OS, stratified by stage at diagnosis and within each stage. Displayed *P* values are nominal two-sided *P* values associated with the observed hazard ratios from the multivariable regression models. Bold numbers indicate *P* values <0.05.

https://doi.org/10.1038/s41591-024-03362-3

Extended Data Table 4 | OS by *KRAS* variant

	G12D/V/R			*All variants*		
Characteristic	**HR[1]**	**95% CI[1]**	**p-value**	**HR[1]**	**95% CI[1]**	**p-value**
KRAS variant			**0.007**			**0.032**
G12D	—	—		—	—	
G12V	0.89	0.79, 1.01	0.061	0.89	0.79, 1.01	0.072
G12R	0.78	0.67, 0.92	**0.003**	0.78	0.66, 0.91	**0.002**
G12C				0.62	0.38, 1.01	0.054
Q61H				0.83	0.64, 1.08	0.17
Q61R				0.93	0.62, 1.39	0.71
Other				0.82	0.61, 1.10	0.19
KRAS mutant allele CN			**2.0e-05**			**5.1e-05**
1	—	—		—	—	
2	1.59	1.30, 1.95	**7.2e-06**	1.52	1.26, 1.84	**1.3e-05**
Indeterminate	1.03	0.92, 1.16	0.61	1.05	0.94, 1.18	0.40
Sex			**2.9e-04**			**2.8e-04**
Male	—	—		—	—	
Female	0.81	0.73, 0.91	**2.9e-04**	0.82	0.74, 0.91	**2.8e-04**
Age at dx	1.01	1.00, 1.01	**0.028**	1.01	1.00, 1.01	**0.007**
Ancestry			**0.001**			**0.007**
EUR	—	—		—	—	
ADMIX/OTHER	1.06	0.87, 1.29	0.54	1.05	0.87, 1.26	0.64
EAS	1.11	0.85, 1.44	0.45	1.07	0.83, 1.38	0.59
AFR	1.14	0.86, 1.51	0.37	1.14	0.86, 1.50	0.35
SAS	2.44	1.60, 3.74	**4.0e-05**	2.06	1.40, 3.04	**2.6e-04**
Time from dx to collection (yr)	1.03	0.97, 1.08	0.35	1.03	0.98, 1.09	0.21
Disease status			**1.2e-10**			**1.9e-12**
Primary	—	—		—	—	
Metastatic	1.98	1.61, 2.44	**1.2e-10**	2.02	1.66, 2.46	**1.9e-12**

[1]HR = Hazard Ratio, CI = Confidence Interval

OS by *KRAS* variant among patients with $KRAS^{MUT}$ tumors with a single *KRAS* variant considered for survival analysis (Methods, n=2,130). Multivariable Cox proportional hazards model of OS, stratified by stage at diagnosis. Displayed *P* values are nominal two-sided *P* values associated with the observed hazard ratios from the multivariable regression models. Bold numbers indicate *P* values <0.05.

https://doi.org/10.1038/s41591-024-03362-3

Extended Data Table 5 | OS by gene-level alterations

	RNF43			*AKT2*			*BRCA2*		
Characteristic	**HR[†]**	**95% CI[†]**	**p-value**	**HR[†]**	**95% CI[†]**	**p-value**	**HR[†]**	**95% CI[†]**	**p-value**
Altered	2.79	1.40, 5.56	**0.004**	2.03	1.26, 3.29	**0.004**	0.66	0.44, 0.98	**0.038**
Sex									
Male	—	—		—	—		—	—	
Female	0.72	0.56, 0.92	**0.009**	0.74	0.58, 0.94	**0.016**	0.74	0.58, 0.95	**0.018**
Age at dx	1.01	1.00, 1.02	0.10	1.01	1.00, 1.02	**0.046**	1.01	1.00, 1.02	0.10
Ancestry									
EUR	—	—		—	—		—	—	
ADMIX/OTHER	1.52	0.97, 2.38	0.066	1.46	0.93, 2.29	0.10	1.43	0.91, 2.23	0.12
EAS	0.95	0.44, 2.01	0.88	1.12	0.53, 2.39	0.76	1.21	0.57, 2.59	0.62
AFR	0.96	0.53, 1.73	0.89	0.93	0.52, 1.68	0.82	1.01	0.56, 1.81	0.98
SAS	1.60	0.78, 3.26	0.20	1.61	0.79, 3.28	0.19	1.49	0.73, 3.04	0.27
Time from dx to collection (yr)	1.36	1.10, 1.68	**0.004**	1.34	1.08, 1.65	**0.007**	1.29	1.04, 1.60	**0.018**

	TP53			*CDKN2A/B*			*SMAD4*			*ARID1A*			*MYC*		
Characteristic	**HR[†]**	**95% CI[†]**	**p-value**	**HR[†]**	**95% CI[†]**	**p-value**	**HR[†]**	**95% CI[†]**	**p-value**	**HR[†]**	**95% CI[†]**	**p-value**	**HR[†]**	**95% CI[†]**	**p-value**
Altered	1.13	0.80, 1.59	0.49	1.24	0.96, 1.60	0.10	0.86	0.66, 1.13	0.28	1.18	0.79, 1.76	0.43	1.52	0.98, 2.37	0.062
Sex															
Male	—	—		—	—		—	—		—	—		—	—	
Female	0.74	0.57, 0.94	**0.015**	0.76	0.59, 0.98	**0.034**	0.73	0.57, 0.94	**0.014**	0.73	0.57, 0.94	**0.014**	0.74	0.58, 0.95	**0.018**
Age at dx	1.01	1.00, 1.02	0.088	1.01	1.00, 1.02	0.078	1.01	1.00, 1.02	0.053	1.01	1.00, 1.02	0.092	1.01	1.00, 1.02	0.11
Ancestry															
EUR	—	—		—	—		—	—		—	—		—	—	
ADMIX/OTHER	1.48	0.94, 2.31	0.088	1.44	0.92, 2.26	0.11	1.48	0.95, 2.31	0.085	1.50	0.96, 2.35	0.076	1.38	0.87, 2.18	0.17
EAS	1.13	0.53, 2.41	0.75	1.19	0.56, 2.52	0.65	1.06	0.50, 2.23	0.89	1.11	0.53, 2.34	0.79	1.11	0.53, 2.34	0.78
AFR	0.98	0.55, 1.76	0.95	1.02	0.57, 1.84	0.94	1.00	0.56, 1.80	>0.99	1.00	0.56, 1.80	>0.99	0.99	0.55, 1.77	0.97
SAS	1.53	0.75, 3.12	0.24	1.52	0.75, 3.10	0.25	1.51	0.74, 3.09	0.25	1.59	0.78, 3.24	0.20	1.61	0.79, 3.28	0.19
Time from dx to collection (yr)	1.31	1.06, 1.62	**0.013**	1.33	1.08, 1.64	**0.008**	1.32	1.07, 1.63	**0.010**	1.33	1.07, 1.64	**0.009**	1.32	1.07, 1.63	**0.010**

	KDM6A			*TGFBR2*			*KMT2C*			*RB1*			*PIK3CA*		
Characteristic	**HR[†]**	**95% CI[†]**	**p-value**	**HR[†]**	**95% CI[†]**	**p-value**	**HR[†]**	**95% CI[†]**	**p-value**	**HR[†]**	**95% CI[†]**	**p-value**	**HR[†]**	**95% CI[†]**	**p-value**
Altered	1.29	0.79, 2.13	0.31	0.66	0.32, 1.35	0.25	0.97	0.50, 1.89	0.92	1.03	0.54, 1.98	0.93	0.71	0.37, 1.35	0.30
Sex															
Male	—	—		—	—		—	—		—	—		—	—	
Female	0.72	0.56, 0.93	**0.011**	0.75	0.58, 0.96	**0.023**	0.73	0.57, 0.94	**0.013**	0.73	0.57, 0.94	**0.013**	0.74	0.58, 0.95	**0.016**
Age at dx	1.01	1.00, 1.02	0.080	1.01	1.00, 1.02	0.076	1.01	1.00, 1.02	0.074	1.01	1.00, 1.02	0.074	1.01	1.00, 1.02	0.056
Ancestry															
EUR	—	—		—	—		—	—		—	—		—	—	
ADMIX/OTHER	1.50	0.96, 2.34	0.077	1.50	0.96, 2.34	0.076	1.49	0.95, 2.33	0.082	1.48	0.94, 2.34	0.090	1.47	0.94, 2.30	0.091
EAS	1.11	0.52, 2.35	0.78	1.09	0.52, 2.29	0.83	1.10	0.52, 2.32	0.81	1.10	0.52, 2.32	0.80	1.08	0.51, 2.29	0.83
AFR	1.01	0.56, 1.81	0.99	1.02	0.57, 1.83	0.95	0.99	0.55, 1.78	0.97	0.99	0.55, 1.78	0.98	0.98	0.55, 1.77	0.96
SAS	1.58	0.77, 3.21	0.21	1.54	0.76, 3.14	0.23	1.55	0.76, 3.16	0.23	1.56	0.76, 3.17	0.22	1.52	0.75, 3.10	0.25
Time from dx to collection (yr)	1.33	1.08, 1.64	**0.008**	1.32	1.07, 1.63	**0.011**	1.32	1.07, 1.63	**0.009**	1.32	1.07, 1.63	**0.009**	1.32	1.07, 1.63	**0.010**

OS by genomic alterations in $n=13$ genes among patients with metastatic disease at diagnosis with $KRAS^{MUT}$ tumors who received first-line chemotherapy considered for survival analysis, limited to high-purity samples (Methods, $n=304$). Multivariable Cox proportional hazards model of OS, stratified by stage at diagnosis. Displayed *P* values are nominal two-sided *P* values associated with the observed hazard ratios from the multivariable regression models. Bold numbers indicate *P* values <0.05.

nature portfolio

Corresponding author(s): Eileen M. O'Reilly, Chaitanya Bandlamudi

Last updated by author(s): 09/12/2024

Reporting Summary

Nature Portfolio wishes to improve the reproducibility of the work that we publish. This form provides structure for consistency and transparency in reporting. For further information on Nature Portfolio policies, see our Editorial Policies and the Editorial Policy Checklist.

Statistics

For all statistical analyses, confirm that the following items are present in the figure legend, table legend, main text, or Methods section.

n/a	Confirmed
☐	☒ The exact sample size (*n*) for each experimental group/condition, given as a discrete number and unit of measurement
☒	☐ A statement on whether measurements were taken from distinct samples or whether the same sample was measured repeatedly
☐	☒ The statistical test(s) used AND whether they are one- or two-sided *Only common tests should be described solely by name; describe more complex techniques in the Methods section.*
☐	☒ A description of all covariates tested
☐	☒ A description of any assumptions or corrections, such as tests of normality and adjustment for multiple comparisons
☐	☒ A full description of the statistical parameters including central tendency (e.g. means) or other basic estimates (e.g. regression coefficient) AND variation (e.g. standard deviation) or associated estimates of uncertainty (e.g. confidence intervals)
☐	☒ For null hypothesis testing, the test statistic (e.g. *F*, *t*, *r*) with confidence intervals, effect sizes, degrees of freedom and *P* value noted *Give P values as exact values whenever suitable.*
☒	☐ For Bayesian analysis, information on the choice of priors and Markov chain Monte Carlo settings
☒	☐ For hierarchical and complex designs, identification of the appropriate level for tests and full reporting of outcomes
☒	☐ Estimates of effect sizes (e.g. Cohen's *d*, Pearson's *r*), indicating how they were calculated

Our web collection on statistics for biologists contains articles on many of the points above.

Software and code

Policy information about availability of computer code

Data collection	Clinical annotations were collected using RedCAP.
Data analysis	Analyses were conducted using R version 4.3.0 with the tidyverse (v2.0.0), rstatix (v0.7.2), stats (v4.3.0), binom (v1.1.1.1), survival (v3.5-5), and gtsummary (v1.7.2) packages, and visualized using ggplot2 (v3.4.4). FACETS v0.5.14 - https://github.com/mskcc/facets OncoKB v4.12 - https://www.oncokb.org cBioPortal v6.0.2 - https://www.cbioportal.org

For manuscripts utilizing custom algorithms or software that are central to the research but not yet described in published literature, software must be made available to editors and reviewers. We strongly encourage code deposition in a community repository (e.g. GitHub). See the Nature Portfolio guidelines for submitting code & software for further information.

Data

Policy information about availability of data

All manuscripts must include a data availability statement. This statement should provide the following information, where applicable:

- Accession codes, unique identifiers, or web links for publicly available datasets
- A description of any restrictions on data availability
- For clinical datasets or third party data, please ensure that the statement adheres to our policy

Our full genomic (somatic) and associated clinical data for all patients in this study will be deposited in cBioPortal for Cancer Genomics and publicly accessible and downloadable alongside this study at publication at: https://www.cbioportal.org/study/summary?id=pdac_msk_2024. Raw tumor and normal sequencing data from MSK-IMPACT are considered protected information, and access to data is available under restricted access subject to additional institutional approvals; these data may be requested for appropriate use from the corresponding authors. Data will be shared for a span of 2 years within 2 weeks of execution of a data transfer agreement with MSK, which will retain all title and rights to the data and results from their use.

Research involving human participants, their data, or biological material

Policy information about studies with human participants or human data. See also policy information about sex, gender (identity/presentation), and sexual orientation and race, ethnicity and racism.

Reporting on sex and gender	Sex is reported in Table 1 and in Supplementary Table 1 and was accounted for in analyses as described in the text.
Reporting on race, ethnicity, or other socially relevant groupings	Inference of genetic ancestry is described in the study methods. Ancestry is reported in Table 1 and Supplementary Table 1 and was accounted for in analyses as described in the text.
Population characteristics	Population characteristics are described in Table 1.
Recruitment	This is a retrospective study; patients were included as part of routine clinical care.
Ethics oversight	Patients were consented to tumor profiling under an institutional IRB-approved research protocol, "Tumor Genomic Profiling in Patients Evaluated for Targeted Cancer Therapy" (NCT01775072).

Note that full information on the approval of the study protocol must also be provided in the manuscript.

Field-specific reporting

Please select the one below that is the best fit for your research. If you are not sure, read the appropriate sections before making your selection.

☒ Life sciences ☐ Behavioural & social sciences ☐ Ecological, evolutionary & environmental sciences

For a reference copy of the document with all sections, see nature.com/documents/nr-reporting-summary-flat.pdf

Life sciences study design

All studies must disclose on these points even when the disclosure is negative.

Sample size	The study investigated a retrospective cohort, comprised of 2,566 pancreatic cancer patients who underwent prospective matched tumor and normal sequencing using our FDA-authorized MSK-IMPACT clinical assay between January 2014 and September 2021.
Data exclusions	As we describe in the methods, we excluded 230 patients due to poor sequencing quality or chart review revealed that patients had a histologic subtype diagnoses other than pancreatic ductal adenocarcinoma.
Replication	No experimental replication was performed.
Randomization	No randomization was performed. Clinical, genomic, and technical covariates were accounted for in the analyses as described in the text.
Blinding	No blinding of data was performed.

Reporting for specific materials, systems and methods

We require information from authors about some types of materials, experimental systems and methods used in many studies. Here, indicate whether each material, system or method listed is relevant to your study. If you are not sure if a list item applies to your research, read the appropriate section before selecting a response.

Materials & experimental systems

n/a	Involved in the study
☒	☐ Antibodies
☒	☐ Eukaryotic cell lines
☒	☐ Palaeontology and archaeology
☒	☐ Animals and other organisms
☐	☒ Clinical data
☒	☐ Dual use research of concern
☒	☐ Plants

Methods

n/a	Involved in the study
☒	☐ ChIP-seq
☒	☐ Flow cytometry
☒	☐ MRI-based neuroimaging

Clinical data

Policy information about clinical studies

All manuscripts should comply with the ICMJE guidelines for publication of clinical research and a completed CONSORT checklist must be included with all submissions.

Clinical trial registration	NCT01775072
Study protocol	The protocol for prospective tumor sequencing of advanced cancers is available at clinicaltrials.gov, NCT01775072. Our study represents a retrospective anlaysis of clinical sequence data generated through that study, which was approved as a retrospective research protocol by the MSK institutional review board (IRB #19-242).
Data collection	The study investigated a retrospective cohort, comprised of 2,566 pancreatic cancer patients who underwent prospective matched tumor and normal sequencing using our FDA-authorized MSK-IMPACT clinical assay between January 2014 and September 2021. Clinical data was curated for 1,480 patients that were seen at MSKCC between January 2014 and March 2021 and had at least one year of clinical follow-up.
Outcomes	Not applicable as this is not a prospective clinical trial.

Plants

Seed stocks	*Report on the source of all seed stocks or other plant material used. If applicable, state the seed stock centre and catalogue number. If plant specimens were collected from the field, describe the collection location, date and sampling procedures.*
Novel plant genotypes	*Describe the methods by which all novel plant genotypes were produced. This includes those generated by transgenic approaches, gene editing, chemical/radiation-based mutagenesis and hybridization. For transgenic lines, describe the transformation method, the number of independent lines analyzed and the generation upon which experiments were performed. For gene-edited lines, describe the editor used, the endogenous sequence targeted for editing, the targeting guide RNA sequence (if applicable) and how the editor was applied.*
Authentication	*Describe any authentication procedures for each seed stock used or novel genotype generated. Describe any experiments used to assess the effect of a mutation and, where applicable, how potential secondary effects (e.g. second site T-DNA insertions, mosiacism, off-target gene editing) were examined.*